Exploring the physicochemical profile and the binding patterns of selected novel anticancer Himalayan plant derived active compounds with macromolecular targets

Arun Bahadur Gurung, Atanu Bhattacharjee, Mohammad Ajmal Ali

www.elsevier.com/locate/imu

PII: S2352-9148(16)30023-5
DOI: http://dx.doi.org/10.1016/j.imu.2016.09.004
Reference: IMU17

To appear in: *Informatics in Medicine Unlocked*

Received date: 19 July 2016
Revised date: 23 September 2016
Accepted date: 23 September 2016

Cite this article as: Arun Bahadur Gurung, Atanu Bhattacharjee and Mohammad Ajmal Ali, Exploring the physicochemical profile and the binding patterns of selected novel anticancer Himalayan plant derived active compounds with macromolecular targets, *Informatics in Medicine Unlocked* http://dx.doi.org/10.1016/j.imu.2016.09.004

Exploring the physicochemical profile and the binding patterns of selected novel anticancer Himalayan plant derived active compounds with macromolecular targets

Arun Bahadur Gurung[a] , Atanu Bhattacharjee[a,]*, Mohammad Ajmal Ali[b]

[a] Computational Biology Laboratory, Department of Biotechnology and Bioinformatics, North Eastern Hill University, Shillong-793022, Meghalaya, India

[b] Department of Botany and Microbiology, College of Science, King Saud University, Riyadh 11451, Saudi Arabia

*Corresponding author: Atanu Bhattacharjee

Mailing Address: Computational Biology Laboratory, Department of Biotechnology and Bioinformatics, North Eastern Hill University, Shillong-793022, India

Tel.: +91 0364-2722406; Fax: +91 364-2550108

Mobile phone: +919436703339

E-mail: atanubioinfo@gmail.com

Title: Exploring the physicochemical profile and molecular interaction of selected novel anticancer Himalayan plant derived active compounds with macromolecular targets

Abstract: Plants are vital source of compounds offering plethora of therapeutic effects against various ailments without much side effects. Due to wide spread prevalence and drug resistance in cancer; there is an urgent need for discovery of new anti-cancer drugs. In the present study, selected novel anti-cancer plants derived compounds (cmpd1 to cmpd15) from Himalayan region were docked with defined molecular targets that regulate cell proliferation and apoptosis. The binding energies of best docked compounds ranged between -8.0 kcal/mol to -11.71 kcal/mol. Further analysis revealed critical hydrogen bonds and hydrophobic interactions between compounds and targets. The best docked compounds viz., cmpd15 against cyclin-dependent kinase-2 (CDK-2), cmpd8 against CDK-6 and cmpd9 against Topoisomerase I and II showed higher binding affinities than the native co-crystal ligands. The root mean square deviation (RMSD) and potential energy plot clearly indicates the stability of the complexes during 20 ns molecular dynamics (MD) simulation. The Molecular Mechanics/Poisson Boltzmann Surface Area (MM/PBSA) binding energy analysis revealed Van der Waals energy component which is the principal stabilizing energy for their interactions except CDK-2/cmpd15 complex. The polar solvation energy did not have favorable contribution to their stabilization. The binding energy decomposition analysis revealed per residue contribution for each docked complexes. Physicochemical profile studies showed that majority of the compounds conform to Lipinski's rule of five (ROF) having low to high blood brain barrier (BBB) penetration, human intestinal absorption, plasma binding protein inhibition and P glycoprotein inhibition.

Keywords: ADMET, anticancer, MM/PBSA, molecular docking, molecular dynamics simulation and plant derived compounds

1. Introduction:

Cancer is the leading cause of deaths worldwide today, which have affected the lives of millions of people around the world. Efforts have been made towards development of new drugs for the prevention and treatment of cancer. The major problem of cancer treatment is the adverse effects of chemotherapy drugs which have been reported to have negative impact in our body and also suppression of the immune system. Besides, the effectiveness of chemotherapy is limited by drug resistance [1,2]. There is an urgent need for new anti-cancer drugs and therapies. Plant derived natural compounds have been in use against various ailments since ancient period and has been regarded as promising drugs against cancer without much of side-effects. A total of 26 plant derived drugs were approved/launched during 2000-2006 [3]. Alkaloids such as vinblastine isolated from *Catharanthus roseus*, is commonly used to treat Hodgkin's lymphoma [4,5]. Camptothecin, another monoterpene indole alkaloid isolated from certain angiosperms have been effective against recurrent colon cancer and its cellular target is DNA topoisomerase I [6,7]. Paclitaxel, a diterpene alkaloid isolated from *Taxus brevifolia* is effective against breast and ovarian cancer and acts by blocking depolymerization of microtubules [8]. Etoposide, a semisynthetic derivative of podophyllotoxin, isolated from roots of *Podophyllum peltatam* has been approved for lung cancer, choriocarcinoma, ovarian cancer, lymphoma etc and its mode of action is through inhibition of DNA topoisomerase II [8].

The rapid advancement of high throughput screening, structural elucidation and combinatorial synthesis have revitalized the potential of plant derived compounds as chemotherapeutic agents against cancer. For developing any natural product for clinical application we need to comprehensively understand and identify its molecular targets and mode of action [9]. Computational screening programs such as molecular docking has greatly helped in rapid screening of chemical entities against their macromolecular targets [10-12]. Besides, in silico toxicity screens have routinely been employed in drug discovery pipelines to study the pharmacokinetic and pharmacodynamics properties of the selected drug-like compounds before proceeding to experimental trials [13].

Recently, fifteen novel Himalayan plant derived compounds have been reported which display anti cancer properties [14]. The present study aims at exploring the binding modes of these fifteen compounds against nine selected molecular targets- CDK-2, CDK-6, Topoisomerase I, DNA Topoisomerase II, Telomere: G-quadruplex, Bcl-2, VEGFR-2, β-tubulin and XIAP

because of their essential role in regulating cellular proliferation and apoptosis [15]. These 15 plant derived compounds belong to different classes of natural compounds. The binding modes of the docked complexes were subjected to molecular dyamics (MD) simulation in order to determine the stability of the system. MM/PBSA binding analysis was performed to determine the driving energy component for molecular interaction and binding per residue contribution. The physicochemical properties of the compounds were determined to explore their bioavailability and possible toxicities in humans.

2. Materials and methods

2.1. *Structure modeling of active compounds*

The structural information of the fifteen selected compounds viz; Acetylshikonin (cmpd1), 5,7,4'-Trimethoxyflavanone (cmpd2), 3-(8'(Z),11'(Z)-pentadecadienyl)catechol (cmpd3), 3,5,6,7,8,3',4'-heptamethoxyflavone (cmpd4), Chrysoplenetin (cmpd5), Chrysosplenol (cmpd6), 1-phenyl-hepta-1,3,5-triyne (cmpd7), Asclepin (cmpd8), 12B-hydroxycalotropin (cmpd9), Solamargine (cmpd10), Taxiresinol (cmpd11), Isotaxirenisol (cmpd12), Secoisolariciresinol (cmpd13), 2-deacetoxytaxinine J (2-DAT-J) (cmpd14) and Asiati cacid (cmpd15) reported to have anti-anticancer properties were retrieved from the review literature [14]. The 2D structures of the fifteen compounds were modeled and converted to 3D structures using ACD/ChemSketch version 12.01 software. These structures were then optimized using MMFF force field, using optimization parameters such as 500 steps of steepest descent algorithm and convergence criterion of 10e-7 [16]. The optimized structures were used for molecular docking studies.

2.2 *Molecular docking studies*

The three dimensional structures of nine selected molecular targets (receptors) involved in regulating cell proliferation and apoptosis- CDK-2(PDB ID: 1DI8), CDK-6(PDB ID: 1XO2), Topoisomerase I (PDB ID: 1T8I), Topoisomerase II (PDB ID: 1ZXM), G-Quadruplex (PDB ID: 1L1H) , Bcl-2(PDB ID: 2O2F), VEGFR-2 (PDB ID: 2OH4), β-Tubulin (PDB ID: 4I4T) and XIAP-Bir2 (PDB ID: 4KJU) were obtained from Protein Data Bank (PDB) (www.rcsb.org). Because of the absence of β tubulin crystal structure in *Homo sapiens* we used *Bos taurus* tubulin as it showed 100 % identity with humans (Chain B of PDB ID: 4I4T). The steps for preparation of receptors include (a) removal of heteroatoms (water, ions), (b) addition of polar hydrogens, and (c) assignment of Kollman charges. The active sites were defined by considering grid boxes of appropriate sizes around the bound co-crystal ligands as shown in Table 1.

The fifteen natural compounds were docked against nine molecular targets using AutoDock4.2 software [17]. Docking experiment was performed using Lamarckian Genetic Algorithm, with an initial population of 250 randomly placed individuals, a maximum number of 10^6 energy

evaluations, a mutation rate of 0.02, and a crossover rate of 0.8. One hundred independent docking runs were performed for each compound. Conformation clustering was done considering root mean square deviation (RMSD) cut-off of 2.0 Å were cluster and the most favorable conformation was represented by the lowest free energy of binding (ΔG) and the lowest inhibition constant (K_i). The most favorable binding conformation was selected and evaluated for molecular interaction with their receptors using LigPlot+ version 1.4.5 software [18]. To ensure that the binding pose of the docked compound represents favorable and valid potential binding mode, the docking parameters and methods were validated by redocking the co-crystal ligand against their respective targets.

2.3. *Molecular dynamics studies*

The trajectories of docked complexes were analyzed through 20 ns of MD simulations using GROMACS 4.6.5 software package [19] with GROMOS96 43a1 force field for protein docked complexes and Amber ff99SB force field for DNA docked complex. The complexes were prepared for MD simulation through solvation within a water filled 3-D cube of 1 Å spacing using simple point charge (SPC216), a three-point model for water. A leap-frog time integration algorithm was used for integrating Newton's equations of motion. The systems were neutralized and energy minimized. The temperature was set at 300 K and the complexes were equilibrated for 100 ps in NVT (Number of particles, Volume and Temperature) ensemble and another 100 ps in NPT ensemble (Number of particles, Pressure and Temperature). After heating and equilibration, the docked complexes were subjected to production MD run for 20 ns in NPT ensemble. PRODRG web server [20] and ACPYPE program [21] was used to generate topologies for ligands compatible with GROMOS96 43a1 force field and Amber ff99SB force field respectively. The particulars of the docked complexes used in MD simulation are enumerated in Table 2. Root mean square deviation (RMSD) and potential energies of the docked complexes was calculated using g_rms and g_energy programs respectively. The graphs are generated using Origin 7.0 software and Xmgrace plotting tools.

2.4. *MM/PBSA binding energy analysis*

The binding free energies of the docked complexes were computed using g_mmpbsa tool of GROMACS software [22] based on the molecular mechanics/Poisson–Boltzman surface area (MM/PBSA) method [23]. The binding energy of the target with the ligand in solvent (ΔG_{bind}) is calculated using equation (Eq. 1):

$$\Delta G_{bind} = G_{complex} - (G_{target} + G_{ligand}) \quad (1)$$

where, $G_{complex}$ is the total free energy of the target-ligand complex and G_{target} and G_{ligand} are total free energies of the target and ligand in solvent, respectively.

The free energy for each individual component can be expressed by equation (Eq. 2)

$$G_X = \langle E_{MM} \rangle - TS + \langle G_{Solv} \rangle \quad (2)$$

where, x is the target or ligand or target−ligand complex. $\langle E_{MM} \rangle$ is the average molecular mechanics potential energy in a vacuum. TS refers to the entropic contribution to the free energy in a vacuum where T and S denote the temperature and entropy, respectively. The last term $\langle G_{Solv} \rangle$ is the free energy of solvation.

The binding free energy calculations were performed for 1000 frames taken at an interval of 10 ps during the equilibrium phase of each trajectory of MD simulation. The average binding energy was computed by using bootstrap analysis method [22].

2.5. *Physicochemical profile of active compounds*

The drug attrition is a serious problem at clinical stages of drug development due to lack of sufficient pharmacokinetics and pharmacodynamics studies. Various physico-chemical properties such as drug-like properties and toxicity of the selected compounds were evaluated using open source tools such as Molinspiration (http://www.molinspiration.com/), DataWarrior program version 3.12.1 software [24], FAF Drugs3 (http://fafdrugs3.mti.univ-paris-diderot.fr/) and PreADMET (https://preadmet.bmdrc.kr/).

3. Results and Discussion

3.1. *Molecular docking analysis*

Before proceeding with docking of selected natural compounds, the docking protocols and parameters were validated by redocking method. The co-crystal ligands viz; DTQ, FSE, EHD, ANP, PYN, LI0, GIG, GDP and 1RH were docked with their cognate molecular targets-CDK-2, CDK-6, Topoisomerase I, Topoisomerase II, G-Quadruplex, Bcl-2, VEGFR-2, β-tubulin and XIAP-Bir2 respectively. The root mean square deviation (RMSD) between the co-crystal and docked conformation was found to be < 2Å except in case of PYN, where it is slightly higher than 2.0 Å (Figure 1). The redocking results confirmed that ligands were bound to their targets very close to the true conformation indicating the reliability of the docking protocols and parameters. Since these co-crystal ligands except GDP are known inhibitor of their respective targets, therefore, binding energies of each plant derived compounds were compared with them to assess their differences in binding affinities. Fifteen anticancer plant derived compounds (Figure 2) belonging to different classes such as Phenolics, Alkynes, Glycosides, Lignans and Terpenes and nine molecular targets were used for the docking studies. Each compound was docked against the macromolecular targets and their binding energies and molecular interactions were investigated in details. The binding energies of all the 15 compounds and the co-crystal ligands are enumerated in Table 3. The molecular interaction of the best docked compound against each target was analyzed in detail.

3.1.1. *Molecular interaction of cmpd15 with CDK-2*

Cmpd15 was best docked with CDK-2 with binding energy of -10.96 kcal/mol and inhibition constant of 9.24 nM. It interacts with CDK-2 through four hydrogen bonds with Ile10, His84, Gln85, Leu298 and hydrophobic interactions with Ala31, Phe82, Leu83, Asp86, Lys89, Gln131 and Leu134 (Figure 3A). Previous report showed that extract of *Centella asiatica* containing Cmpd15 as active compound exhibited 95% inhibition against MCF-7 cell lines at concentration of 10µg/ml [25] and anti-proliferative effects on multiple myeloma RPMI 8226 cells with IC_{50} values ranging from 53.76 to 24.88µmol/l from 12 to 48 hours respectively [26]. In our molecular docking studies, cmpd15 exhibited better binding energy and displayed stronger interaction with CDK-2 than co-crystal ligand (DTQ). CDK-2 is a critical enzyme regulating the

transition of cells from G1 to S phase. The inhibition of this enzyme therefore, could lead to arrest of cell proliferation in cancer conditions.

3.1.2. *Molecular interaction of cmpd8 with CDK-6*

Cmpd8 was identified as the best docked compound against CDK-6, an enzyme which forms complex with cyclin D and controls the cell cycle progression from G1 to S phase. Cmpd8 displayed binding energy of -11.09 kcal/mol and inhibition constant of 7.48 nM. Its interaction with CDK-6 was comparatively stronger than the co-crystal ligand (FSE), and interacts through six hydrogen bonds with His100, Asp104, Lys147, Asn150 and Asp163 and hydrophobic interactions with Ile19, Gly20, Gly22, Val27, Val101, Asp102, Gln103, Gln149 and Leu152 (Figure 3B). Earlier report showed that the isolated bioactive compound cmpd8 from *Asclepias curassavica* showed IC_{50} of 0.02 mg/ml against human hepatoma carcinoma cell line [27].

3.1.3. *Molecular interaction of cmpd9 with Topoisomerase I, Topoisomerase II, Bcl-2, VEGFR-2 and XIAP-Bir2*

Interestingly, cmpd9 showed best interactions with five macromolecular targets viz; Topoisomerase I, Topoisomerase II, Bcl-2, VEGFR-2 and XIAP-Bir2. It interacts with Topoisomerase I with binding energy of -10.87 kcal/mol and inhibition constant of 10.69 nM. This interaction was comparatively stronger than the co-crystal ligand, and encompasses three hydrogen bonds through Lys425, Tyr426 and Met428 and hydrophobic interactions via Ala351, Asn352, Ile427, Leu429, Pro431, Lys436, Lys439 and Asp440 (Figure 3C). Earlier report showed that the isolated bioactive compound cmpd9 from *Asclepias curassavica* showed IC_{50} of 0.69 mg/ml against human hepatoma carcinoma cell line [27]. This compound showed strong interaction with Topoisomerase I, an enzyme which cleaves one of the strands of double stranded DNA and reanneals the strand. Cmpd9 interacts with Topoisomerase II with binding energy of -11.71 kcal/mol and inhibition constant of 2.63 nM. Topoisomerase II cleave both the stands of double standed DNA to resolve supercoils This interaction was comparatively stronger than the co-crystal ligand, and encompasses five hydrogen bonds through Ser149, Arg162, Asn163 and Gly166 and hydrophobic interactions via Asn91, Arg98, Ile125, Pro126, Ile141, Thr147, Ser148, Asn150, Gly161, Gly164, Tyr165, Ala167 and Gln376 (Figure 3D). Cmpd9 interacts with Bcl-2 with binding energy of -9.46 kcal/mol and inhibition constant of 117.15 nM. B-cell lymphoma-2

(Bcl-2) belongs to Bcl-2 family which inhibits apoptosis. This interaction was comparatively stronger than the co-crystal ligand, and encompasses only hydrophobic interactions via Ala97, Asp100, Phe101, Tyr105, Asp108, Phe109, Met112, Leu134, Gly142, Arg143, Val145, Ala146 and Tyr199 (Figure 3F). Cmpd9 interacts with VEGFR-2 with binding energy of -10.72 kcal/mol and inhibition constant of 13.76 nM. This interaction was comparatively stronger than the co-crystal ligand, and encompasses only hydrophobic interactions via Leu838, Val846, Ala864, Lys866, Glu883, Leu887, Val897, Val914, Glu915, Phe916, Cys917, Gly920, Leu1033, Cys1043, Asp1044 and Phe1045 (Figure 3G).Vascular endothelial growth factor receptor (VEGFR) regulate homeostasis, blood and lymphatic vessel development. Cmpd9 was also best docked with XIAP-Bir2 with binding energy of -8.34 kcal/mol and inhibition constant of 773.40 nM. The X-linked inhibitor of apoptosis protein (XIAP) belongs to IAP family and strong inhibitor of the caspase. This interaction was comparatively stronger than the co-crystal ligand, and encompasses two hydrogen bonds through Lys206 and Lys208 and hydrophobic interactions via Gln197, Leu207, Asn209, Trp210, Glu211, Asp214, Glu219, Arg222 and His223 (Figure 3I).

3.1.4. *Molecular interaction of cmpd12 with G-quadruplex DNA*

G-quadruplex are DNA sequences containing simple guanine- rich tandem repeats at the ends of eukaryotic chromosomes, which maintain genomic stability. Cmpd12 was best docked with G-quadruplex with binding energy of -8.18 kcal/mol and inhibition constant of 1010 nM. This interaction was comparatively stronger than the co-crystal ligand, and encompasses one hydrogen bond through Dg2012 and hydrophobic interactions via Dt1006, Dt1007, Dt1008, Dg1009 and Dg2011 (Figure 3E). Isotaxirenisol (cmpd12) showed inhibition against Caco-2 cell line at IC_{90} of 0.251 µg/ml [28].

3.1.5. *Molecular interaction of cmpd4 with β-tubulin*

Cmpd4 was best docked with β-tubulin with binding energy of -10.87 kcal/mol and inhibition constant of 10.69 nM. β-tubulin is a structural unit of microtubules that regulates cell growth and motility. This interaction was comparatively stronger than the co-crystal ligand, and encompasses three hydrogen bonds through Gln11 and Cys12 and hydrophobic interactions via Ala9, Gly10, Asp69, Glu71, Gly98, Ala99, Asn101, Ser140, Thr145, Gly146, Asp179, Asn206 and Tyr224 (Figure 3H). The ethanolic extract of Citrus limon's fruit containing 3,5,6,7,8,3',4'-

heptamethoxyflavone displayed anticancer activity by inhibiting HT-29 cell line at IC_{50} (5.9 μg/ml) [29] and 3,5,6,7,8,3',4'-heptamethoxyflavone extracted from peel of citrus plants exhibited impressive anti-tumour properties on mouse skin papillomas induced by (±)-(E)-methyl-2-[(E)-hydroxyimino]- 5-nitro-6-methoxy-3-hexenamide (NOR1) [30].

3.2. *Molecular Dynamics simulation analysis*

3.2.1. *System stability of docked complexes*

Each of the nine docked complexes obtained through molecular docking was subjected to molecular dynamics simulation in order to validate the binding modes of the ligands. The snapshots from 0-20 ns time frame trajectories of the docked complexes are represented in Figure 4 which shows the dynamic nature of the target and their bound ligands. Root mean square deviation (RMSD) of Cα atoms of proteins and backbone of G-quadruplex was calculated by superimposing the MD production trajectories to their starting structures in order to evaluate their backbone stability with time. The RMSD values of the docked complexes fluctuated with larger amplitude in the beginning and seemed to remain virtually constant after 10 ns averaging at 0.275±0.012 nm, 0.261±0.042 nm, 0.697±0.048 nm, 0.339±0.019 nm, 0.403±0.014 nm, 0.331±0.012 nm, 0.366±0.018 nm, 0.251±0.010, 0.261±0.017 nm for CDK-2/cmpd15, G-quadruplex/cmpd12, Topoisomerase I/cmpd9, CDK-6/cmpd8, Topoisomerase II/cmpd9, Bcl-2/cmpd9, VEGFR-2/cmpd9, β-tubulin/cmpd4 and XIAP-Bir2/cmpd9 respectively (Figure 5). This confirmed that the complexes had achieved their structural convergence from 10 ns onwards and advocates our choice for considering the time period of MD simulation till 20 ns for various analyses. Larger fluctuation in amplitudes was found for Topoisomerase I/cmpd9 and Topoisomerase II/cmpd9 docked complexes compared to other complexes in this study. Our findings corroborates with recent studies by Singh et al. [31] who has reported higher RMSD value ranging from 0.69-0.7 nm for Topoisomerase I complexed with topotecan (known inhibitor) and oliveroline (alkaloid) and 0.49-0.52 nm for Topoisomerase II complexed with etoposide and oliveroline which seemed to be due to higher flexibility of the protein.

The energetics of the fluctuations of the docked complexes was assessed by monitoring their potential energies during the course of MD simulation which showed steady values reconfirming the stability of the docked complexes (Figure 6). The average potential energies of the docked complexes are -865.886 ±0.767 $\times 10^3$kJ/mol, -209.563±0.350$\times 10^3$kJ/mol, -2871.333±1.379$\times 10^3$

kJ/mol, -893.882±0.775×10^3kJ/mol, -1361.359±0.960×10^3kJ/mol, -403.658±0.513×10^3kJ/mol, -869.709±0.753×10^3 kJ/mol, -930.065±0.788×10^3 kJ/mol, -352.641±0.490×10^3 kJ/mol for CDK-2/cmpd15, G-quadruplex/cmpd12, Topoisomerase I/cmpd9, CDK-6/cmpd8, Topoisomerase II/cmpd9, Bcl-2/cmpd9, VEGFR-2/cmpd9, β-tubulin/cmpd4 and XIAP-Bir2/cmpd9 respectively. The larger negative potential energies of Topoisomerase I and Topoisomerase II docked complexes strongly corroborates with their higher RMSD values in our studies, underlining the greater conformational flexibilities of these proteins.

3.2.2. *Binding Free energy analysis*

To characterize the strength of interaction of best docked ligands with their targets, the binding free energies of the docked complexes were calculated using MM/PBSA methodology considering a total of thousand frames from the last 10 ns of MD production simulation trajectories as shown in Table 4. The binding energies were decomposed into their energy components viz; Van der Waals energy, electrostatic energy, polar solvation energy and SASA non-polar solvation energy to get insights into their individual contributions. In all the docked complexes, the principle driving component of binding being Van der Waals energy except in case of CDK-2/cmpd15 complex, where electrostatic energy component played vital in strengthening the binding mode. The polar solvation energy did not have favorable contribution to the total interaction in all the docked complexes and SASA non-polar solvation energy contribute significantly to their overall binding energies except CDK-2/cmpd15, which may be explained by their decreased Van der Waals energy value due to nonpolar amino acids. Contrary to molecular docking results, the binding mode of cmpd9 did not show favourable interaction with Bcl-2 which may be attributed to decrease contribution by Van der Waals energy, electrostatic energy and SASA non-polar solvation energy.

3.2.3. Residue wise contribution analysis of the docked complexes

The binding energies of the docked complexes were decomposed to explore residue wise contribution to the binding energy (Figure 7 and Table 5). In the CDK-2/cmpd15 complex, the residues dominantly contributing to the binding energy include Arg214, Arg217, Lys237, Arg200, Lys242, Arg169, Arg245, Arg199, Arg274, Lys178 and Lys88. These contributing

polar charged residues substantiates that electrostatic energy component is the driving component of interaction of cmpd15 with CDK-2.

In the CDK-6/cmpd8, residues contributing significantly to the binding energy include Ile19, Glu61, Leu152, Asn150, Asp102, Gln149 and Glu99. The residues Ile19, Leu152, Asn150, Asp102 and Gln149 besides higher contribution are also involved in molecular interaction with cmpd8 as revealed by our molecular docking results.

In the Topoisomerase I/cmpd9, residues contributing to the binding energy include Lys443, Lys439, Met428, Lys425 and Pro431. The residues Lys439, Met428, Lys425 and Pro431 also are involved in molecular interaction with cmpd9 corroborating with the molecular docking results.

In the Topoisomerase II/cmpd9, residues contributing to the binding energy include Ser149, Ile141, Arg162, Ile125 and Val137. The residues Ser149, Ile141, Arg162 and Ile125 are also involved in molecular interaction with cmpd9 which is in agreement with molecular docking results.

In the G-quadruplex/cmpd12 complex, nucleotides contributing to the binding energy include Dt1007, Dg2012, Dg1009, Dt1008, Dg2011, Dt1006 and Dg1010. The nucleotides Dt1007, Dg2012, Dg1009, Dt1008, Dg2011, Dt1006 and Dg1010 are also involved in molecular interaction with cmpd12.

In the Bcl-2/cmpd9 complex, residues contributing to the binding energy include Tyr199, Tyr105, Phe101, Leu198 and Asp100. The residues Tyr199, Tyr105, Phe101 and Asp100 are also involved in molecular interaction with cmpd9.

In the VEGFR-2/cmpd9complex, residues contributing to binding energy include Phe1045, Phe916, Leu838, Tyr1057, Val914, Cys1043, Val897, Leu1033 and Phe919. The residues Phe1045, Phe916, Leu838, Val914, Cys1043, Val897 and Leu1033 are also involved in molecular interaction with cmpd9.

In the β-tubulin/cmpd4 complex, residues contributing to binding energy include Tyr224, Gly142, Cys12, Gly143 and Gln11. The residues Tyr224, Cys12 and Gln11 are also involved in molecular interaction with cmpd9 as indicated before by molecular docking results.

In the XIAP-Bir2/cmpd9 complex, residues contributing to the binding energy include Asn209, Phe224, Lys208, Leu207 and His223. Interestingly, Asn209, Lys208, Leu207 and His223 are also residues involved in interaction with cmpd9 as revealed by molecular docking studies.

3.3. Analysis of physicochemical properties

The physicochemical properties and ADMET properties of fifteen compounds were analyzed using various *in silico* tools realizing the drug attrition rate at later stages of drug development process. The Molinspiration results show that out of fifteen natural compounds selected in our studies, five compounds did not conform to Lipinski's rule of five and exhibit various degrees of violations (Table 6). Lipinski's rule of five (ROF) [32] is a rule of thumb in pharmaceutical science to evaluate the druglikeness and their oral bioavailability in humans based on some criteria- Molecular weight (MW) < 500, compound's lipophilicity expressed as logP (partition coefficient between n-octanol and water) < 5, number of groups in the molecule that can donate hydrogen atoms to form hydrogen bonds (HBD) < 5 and number of groups in the molecule which can accept hydrogen atoms to form hydrogen bonds (HBA) < 10. Compounds -Cmpd3, Cmpd8 and Cmpd9 showed one violation as their LogP and MW were higher than the acceptable range which indicates that Cmpd 3 is highly lipophilic and therefore, may have poor absorption rate. Cmpd 8 and Cmpd9 owing their large molecular weights may limit their diffusion across the biological membranes. Cmpd14 showed two violations with its LogP and MW not within the permissible limit and therefore, may have poor absorption and slow diffusion across the lipid bilayer. Cmpd10 showed the highest degree of violations with 3 violations in its MW, HBA and HBD not within the acceptable range and this may severely limit its diffusion owing to its large molecular weight. This could also affect its permeability due to its greater number of hydrogen bond donor and acceptor groups.

Careful examination of the pharmacokinetic properties of drug-like compounds such as Adsorption, Distribution, Metabolism and Excretion (ADME) in humans can also limit the chance of failures in clinical phases. For this, some physicochemical properties such as polar surface area (sum of surface area of nitrogen and oxygen plus hydrogen atoms attached to heteroatoms) (PSA < 140 $Å^2$), rotatable bonds (RB < 10), aqueous solubility at 25^o and pH=7.5 (LogS > -4.0), Duglikeness, mutagenicity, Tumorigenicity, reproductive effective was evaluated using DataWarrior program (Table 7). The DataWarrior results showed six compounds (Cmpd3, Cmpd7, Cmpd8, Cmpd10, Cmpd14 and Cmpd15) possess LogS value out of the acceptable range, which indicates that these compounds will have low aqueous solubility which in turn will affect their distribution characteristics. Compound cmpd3 and cmpd14 have rotatable bonds out

of the acceptable range which indicates their poor oral bioavailability. Compounds-cmpd9 and cmpd10 have PSA values out of the permissible limit which implies that they may have poor oral bioavailability. The druglikeness score of majority of the compounds have negative score and only three compounds (cmpd4, cmpd6 and cmpd10) possess positive score. Compounds-cmpd 4, cmpd6 and cmpd10 therefore, possess molecular fragments typically present in the marketed drugs. The majority of the compounds except cmpd3, cmpd7 and cmpd14 are non-mutagenic, non-tumerigenic, non irritant and without side effects on the reproductive health. Compounds-cmpd3, cmpd7 and cmpd14 showed high irritant, high tumorigenicity and high irritancy respectively.

Other physicochemical properties of the compounds such as oral bioavailability were evaluated using VEBER rule (a compound possess good oral bioavailability if ≤10 RB and PSA≤140Å^2) and EGAN rule (good orally available compounds have -1≤LogP≤5.8, PSA≤130Å^2), Phospholipidosis and Fsp3 (defines molecular complexity, number of sp3 hybridized carbons/total carbon count). The FAF3 drugs results showed all the compounds have good bioavailability conforming to both VEBER as well as EGAN rule (Table 8). All compounds except cmpd10 are non inducer of phospholipidosis. The compounds -cmpd3, cmpd8, cmpd9, cmpd10, cmpd14 and cmpd15 have impressive Fsp^3 value which may correlate to their good solubility.

PreADME was also used to assess ADMET properties such as, blood brain barrier penetration, human intestinal absorption, CYP_2C19_inhibition, Pgb inhibition and Plasma protein binding based on given criteria (Table 9). Drugs *in vivo* can either bind reversibly to proteins and lipids in plasma known as Plasma protein binding, which is used to monitor drug concentration in clinical trials and predict their therapeutic dose. Plasma protein binding analysis was carried out based on the criteria- a) Chemicals strongly bound with a score more than 90% and b) chemicals weakly bound with a score less than 90%. Our results showed that cmpd3, cmpd7, cmpd12, cmpd14 and cmpd15 are strongly bound to plasma protein binding. Blood-brain barrier (BBB) form a highly selective barrier between the brain and the rest of the body and drugs that target central nervous system (CNS) should have better BBB penetration and drugs that target peripheral organs should have low BBB penetration to minimize side effects to CNS Blood brain barrier penetration were based on the following criteria a) High absorption to CNS for BB> 2.0 b) Middle absorption to CNS for BB between 2.0 to 0.1 c) low absorption to CNS for BB < 0.1

and the results showed that cmpd2, cmpd3 and cmpd7 may have high absorption to CNS. The prediction of human intestinal absorption (HIA) play important role in design, optimization and selection of oral drugs and was evaluated based on the following criteria a) Poorly absorbed compounds for HIA between 0-20% b) Moderately absorbed compounds for HIA between 20-70% and c) well absorbed compounds for HIA between 70-100%. All the compounds have well human intestinal absorption and compd10 is moderately absorbed. Majority of the compounds except cmpd8, cmpd9, cmpd10, cmpd15 were found to inhibitor of CYP_2C19, a Cytochrome P450 (CYP) enzyme, responsible for metabolism of known drugs in humans. It was also revealed that most of the compounds except cmpd3, cmpd4, cmpd8, cmpd10, cmpd14, cmpd15 were found to be non-inhibitor of P-glycoprotein (Pgb). P-glycoprotein is a member of ATP-binding cassette superfamily of membrane transport proteins responsible for efflux of many drugs and is a major component of BBB.

Thus, the physicochemical profile study showed that the best docked compounds- cmpd4, cmpd12 and cmpd15 do not violate ROF except cmpd8 and cmpd9 which showed only one ROF violation, which is acceptable for oral bioavailability. Besides conforming to ROF, they also seem to be non-mutagenic, non-irritant, non-tumorigenic and without any adverse effects on the reproductive effect. They also seem to have good oral bioavailability, non inducer of phospholipidosis, least BBB penetrability and well human intestinal absorption. They are likely to be non CYP_2C19 inhibitor except for compounds-cmpd4 and cmpd12. But, they were found to be Pgp inhibitor except cmpd9 and cmpd12. Except for cmpd12 and cmpd15, others are likely to be weakly bound to plasma proteins. However, these physicochemical properties can be improved by structural modifications using structure activity relationship approach.

4. Conclusion

Realizing the potential of plant derived compounds to develop as drugs against cancer, information on novel anti-cancer compounds from Himalayan region were retrieved from literature. The chemical structures of fifteen such anti-cancer compounds were modeled and optimized and their binding patterns were explored against nine selected molecular targets implicated in cell proliferation and apoptosis, which provided insights into their molecular mechanism of inhibition. Molecular docking results revealed their binding modes with the targets through hydrogen bond and hydrophobic interactions. The compounds which showed

strong interaction with their respective target includes- cmpd15 against CDK-2, cmpd8 against CDK-6, cmpd9 against Topoisomerase I, Topoisomerase II, Bcl-2, VEGFR-2 and XIPA-Bir2, cmpd12 against G-Quadruplex DNA and cmpd4 against β-tubulin. The best docked compounds against each target showed stability in terms of RMSD and potential energy during the entire course of molecular dynamic simulation and MM/PBSA analysis revealed Van der Waals energy as the principal stabilizing energy component of the complexes. The binding energy per residue/nucleotide contribution revealed critical residues/nucleotides contributing significantly to the total binding energy. Physico-chemical profiling of the compounds showed that majority of them have acceptable physicochemical properties conforming to ROF and exhibited low to high BBB penetration, Human intestinal absorption, Plasma binding protein and P glycoprotein inhibition. The present study has great relevance in area of rational drug design such as target fishing for novel compounds and drug optimization for improving their target selectivity and oral bioavailability.

Disclosure statement

The authors declare that they have no competing interests.

Acknowledgement

The author ABG is thankful to the Department of Biotechnology, GOI for providing DBT-Junior Research Fellowship (DBT/JRF/13/AL/4294104). The authors are thankful to DST-FIST (Level1, Sanction No. SR/FST/LSI-443/2010(c)) for providing the financial support for the study.

References

[1] Gottesman MM. Mechanisms of cancer drug resistance. Annu Rev Med 2002;53:615-27.

[2] Holohan C, Van Schaeybroeck S, Longley DB, Johnston PG. Cancer drug resistance: an evolving paradigm. Nat Rev Cancer 2013;13:714-26.

[3] Saklani A, Kutty SK. Plant-derived compounds in clinical trials. Drug Discov Today 2008;13:161-71.

[4] Rowinsky EK, Donehower RC. Paclitaxel (taxol) N Engl J Med 1995;332:1004–14.

[5] Moudi M, Go R, Yien CYS, Nazre M. Vinca Alkaloids. Int J Prev Med 2013;4:1231–5.

[6] Wall ME, Wani MC. Camptothecin and taxol: from discovery to clinic. J Ethnopharmacol 1996;51:239–54.

[7] Hsiang YH, Hertzberg R, Hecht S, Liu LF. Camptothecin induces protein-linked DNA breaks via mammalian DNA topoisomerase I. J Biol Chem 1985;260:14873-78.

[8] Demain AL, Vaishnav P. Natural products for cancer chemotherapy. Microb Biotechnol 2011;4:687-99.

[9] Krysiak J, Breinbauer R. Activity-based protein profiling for natural product target discovery. Top Curr Chem 2012;324:43-84.

[10] Selvam C, Jachak SM, Thilagavathi R, Chakraborti AK. Design, synthesis, biological evaluation and molecular docking of curcumin analogues as antioxidant, cyclooxygenase inhibitory and anti-inflammatory agents. Bioorg Med Chem Lett 2015;15:1793-7.

[11] Yadav DK, Mudgal V, Agrawal J, et al. Molecular docking and ADME studies of natural compounds of Agarwood oil for topical anti-inflammatory activity. Curr Comput Aided Drug Des 2013;9:360-70.

[12] Arun Y, Saranraj K, Balachandran C, Perumal PT. Novel spirooxindole–pyrrolidine compounds: Synthesis, anticancer and molecular docking studies. Eur J Med Chem 2014;74:50-64.

[13] Ntie-Kang F. An in silico evaluation of the ADMET profile of the StreptomeDB database. Springerplus 2013;2:353.

[14] Tariq A, Mussarat S, Adnan M. Review on ethnomedicinal, phytochemical and pharmacological evidence of Himalayan anticancer plants. J Ethnopharmacol 2015;164:96-119.

[15] Phosrithong N, Ungwitayatorn J. Molecular docking study on anticancer activity of plant-derived natural products. Med Chem Res 2010;19:817-35.

[16] Halgren TA. Merck molecular force field. I. Basis, form, scope, parameterization, and performance of MMFF94. J Comput Chem 1996;17:490-519.

[17] Morris GM, Huey R, Lindstrom W, et al. AutoDock4 and AutoDockTools4: Automated docking with selective receptor flexibility. J Comput Chem 2009;30:2785-91.

[18] Laskowski RA, Swindells MB. LigPlot+: multiple ligand–protein interaction diagrams for drug discovery. J Chem Inf Model 2011;51:2778-86.

[19] Hess B, Kutzner C, Van Der Spoel D, Lindahl E. GROMACS 4: algorithms for highly efficient, load-balanced, and scalable molecular simulation. J Chem Theory Comput 2008; 4:435-47.

[20] SchuÈttelkopf AW, Van Aalten DM. PRODRG: a tool for high-throughput crystallography of protein–ligand complexes. Acta Crystallogr D Biol Crystallogr 2004;60:1355-63.

[21] Sousa da Silva AW, Vranken WF. ACPYPE-Antechamber python parser interface. BMC Res Notes 2012;5:367.

[22] Kumari R, Kumar R, Lynn A. g_mmpbsa--a GROMACS tool for high-throughput MM-PBSA Calculations. J Chem Inf Model 2014;54:1951-62.

[23] Kollman PA, Massova I, Reyes C, et al. Calculating structures and free energies of complex molecules: combining molecular mechanics and continuum models. Acc Chem Res 2000;33:889-97.

[24] Sander T, Freyss J, von Korff M, Rufener C. DataWarrior: an open-source program for chemistry aware data visualization and analysis. J Chem Inf Model 2015;55:460-73.

[25] Babykutty S, Padikkala J, Sathiadevan, PP, et al. Apoptosis induction of Centella asiatica on human breast cancer cells. Afr J Tradit Complement Altern Med 2008;6:9-16.

[26] Zhang J, Ai L, Lv T, et al. Asiatic acid, a triterpene, inhibits cell proliferation through regulating the expression of focal adhesion kinase in multiple myeloma cells. Oncol Lett 2013;6:1762-6.

[27] Li JZ, Qing C, Chen CX, et al. Cytotoxicity of cardenolides and cardenolide glycosides from Asclepias curassavica. Bioorg Med Chem Lett 2009;19:1956-9.

[28] Chattopadhyay SK, Kumar TR, Maulik PR, et al. Absolute configuration and anticancer activity of taxiresinol and related lignans of Taxus wallichiana. Bioorg Med Chem 2003;11:4945-8.

[29] Nair PK, Melnick SJ, Wnuk SF, et al. Isolation and characterization of an anticancer catechol compound from Semecarpus anacardium. J Ethnopharmacol 2009;122:450-6.

[30] Iwase Y, Takemura Y, Ju-ichi M, et al. Cancer chemopreventive activity of 3, 5, 6, 7, 8, 3′, 4′-heptamethoxyflavone from the peel of citrus plants. Cancer Lett 2001;163:7-9.

[31] Singh S, Das T, Awasthi M, et al. DNA topoisomerase-directed anticancerous alkaloids: ADMET-based screening, molecular docking, and dynamics simulation. Biotechnol Appl Biochem 2016;63:125-37.

[32] Lipinski CA. Lead-and drug-like compounds: the rule-of-five revolution. Drug Discov Today Technol 2004;1:337-41.

Figure legends

Figure 1: Validation of molecular docking results. The root mean square deviation (RMSD) was calculated between the original co-crystal position (purple) and docked poses (cyan) for the co-crystal ligands DTQ through 1RH.

Figure 2: Chemical structure of fifteen anticancer compounds selected for molecular docking studies belonging to different classes- cmpd1-6 (Phenolics), cmpd7 (Alkyne), cmpd8-10 (Glycosides), cmpd11-13 (Lignans), cmpd14-15 (Terpenes).

Figure 3: LigPlot+ results for molecular interaction of best docked ligands (purple ball and stick) with their molecular targets (A) CDK-2 (B) CDK-6 (C) Topoisomerase I (D) Topoisomerase II (E) G-quadruplex (F) Bcl-2 (G) VEGFR-2 (H) β-tubulin (I) XIAP-Bir2. The green dashed line indicates hydrogen bond with the labeled distance. The arcs with spikes radiating out corresponds to residues involved in hydrophobic interactions.

Figure 4: The snapshots of trajectories of the docked complexes from 0 to 20 ns MD simulation. The protein targets are displayed in ribbon (orange: helix, cyan: sheet, grey: loops), G-quadruplex in strands (tan: backbone, blue: nucleotides) complexed with the best docked ligands in spheres.

Figure 5: The root mean square deviation (RMSD) vs time plot for the trajectories of the nine docked complexes.

Figure 6: The potential energy vs time plot for the trajectories of the nine docked complexes.

Figure 7: MM/PBSA binding free energy contribution on a per residue/ nucleotide basis for each docked complexes.

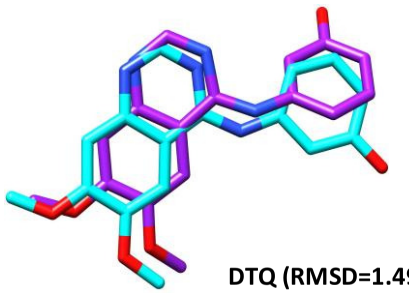

DTQ (RMSD=1.491Å)

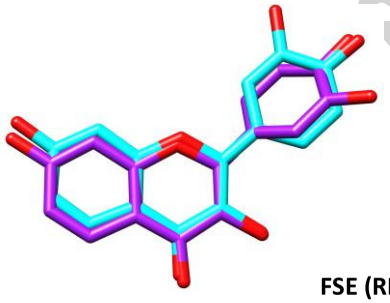

FSE (RMSD=0.713Å)

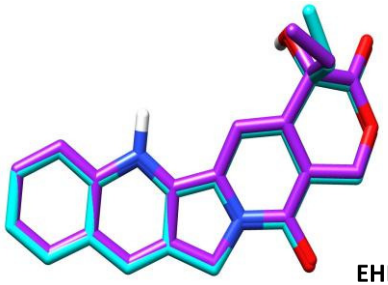

EHD (RMSD=0.218Å)

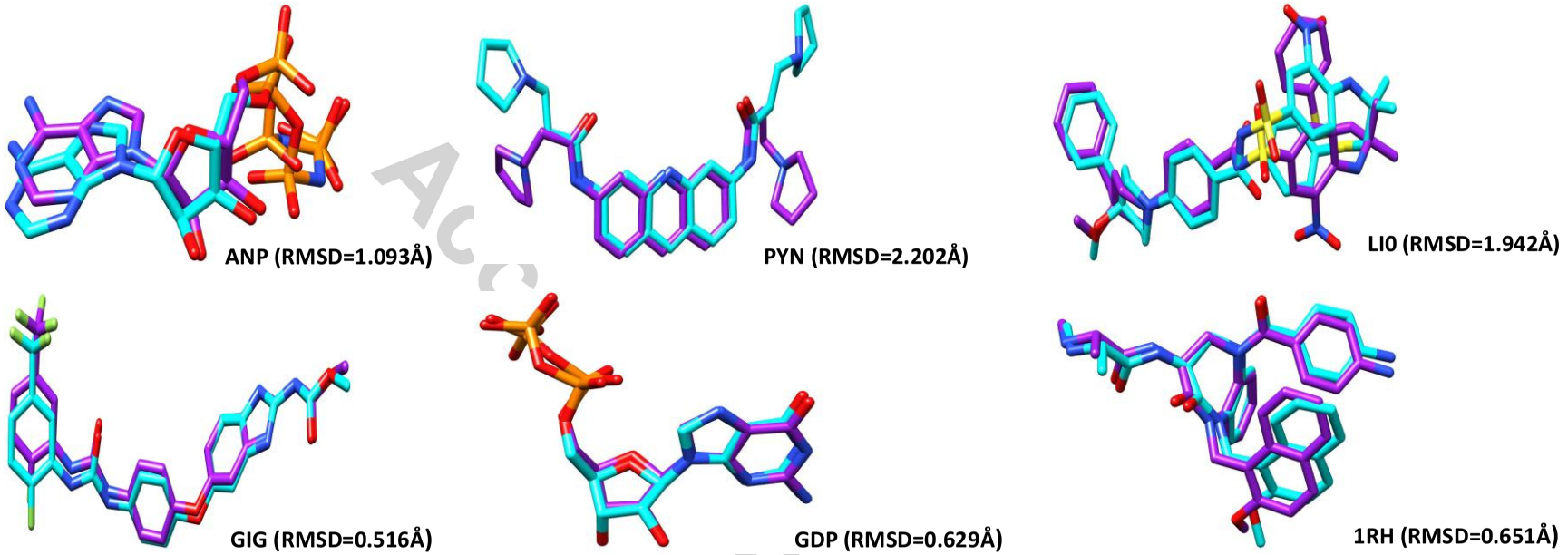

Figure 1

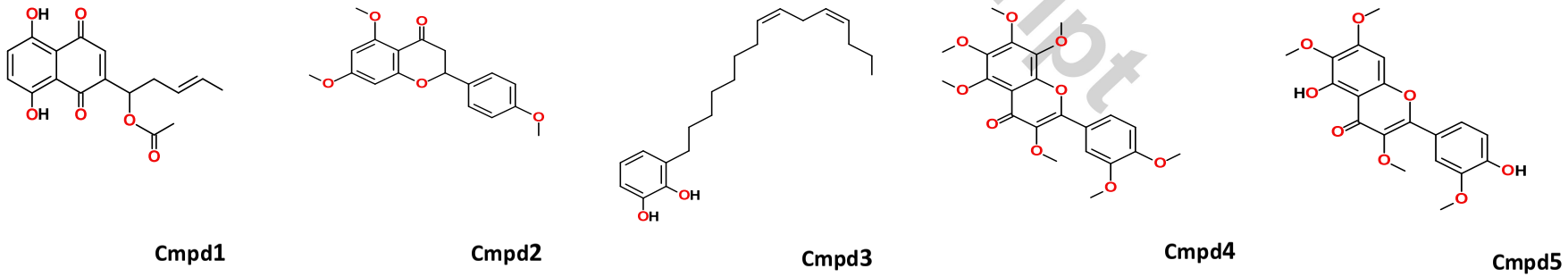

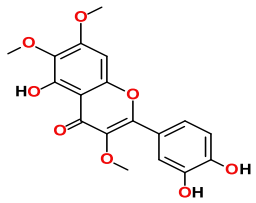

Cmpd6

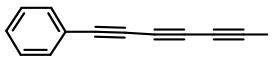

Cmpd7

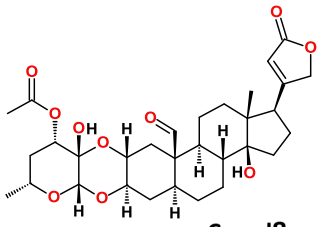

Cmpd8

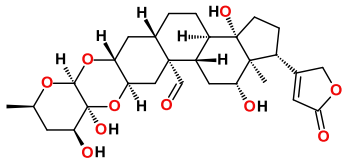

Cmpd9

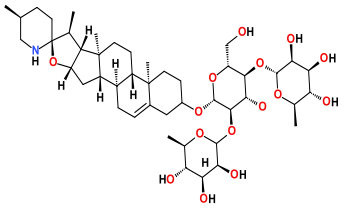

Cmpd10

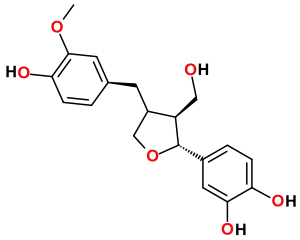

Cmpd11

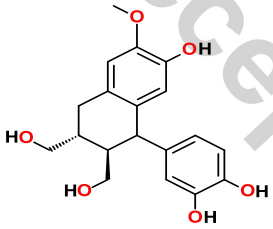

Cmpd12

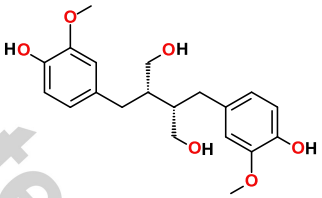

Cmpd13

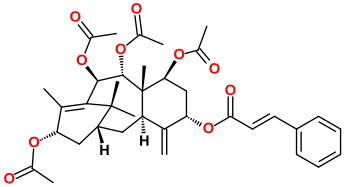

Cmpd14

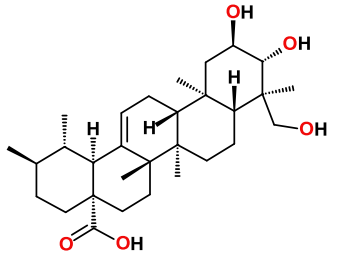

Cmpd15

Figure 2

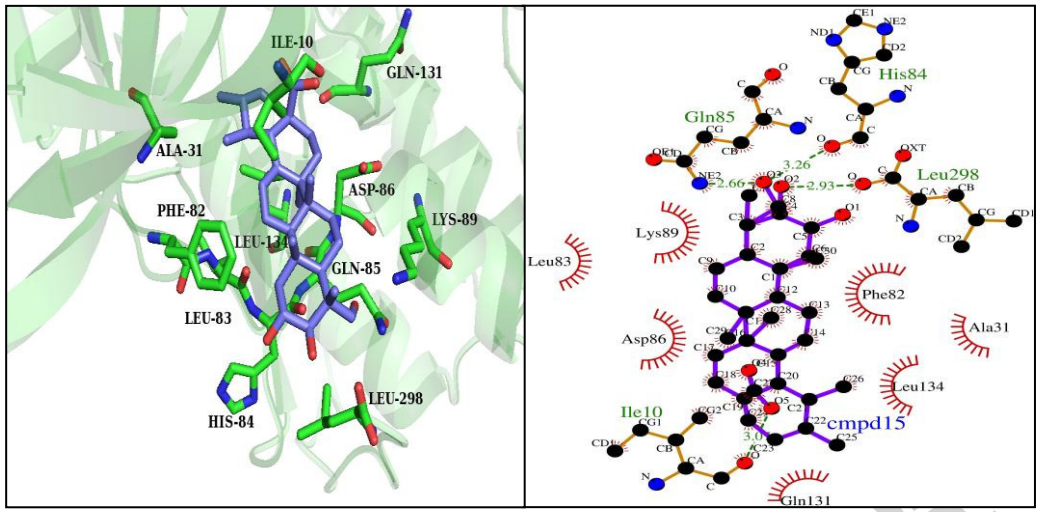
ILE-10
GLN-131
ALA-31
ASP-86
PHE-82
LYS-89
LEU-174
GLN-85
LEU-83
LEU-298
HIS-84
His84
Gln85
Leu298
Lys89
Leu83
Phe82
Asp86
Ala31
Leu134
Ile10
cmpd15
Gln131

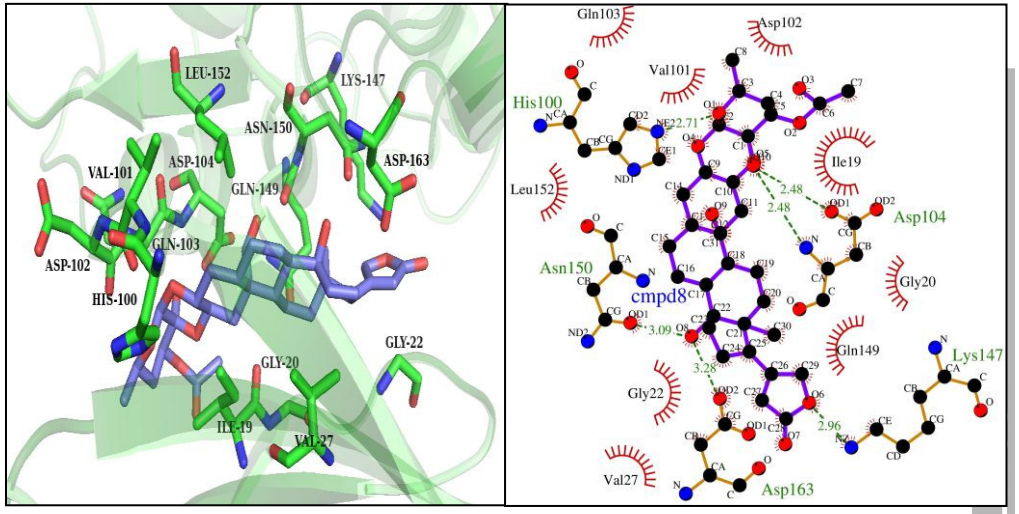
LEU-152
LYS-147
ASN-150
ASP-104
ASP-163
VAL-101
GLN-149
GLN-103
ASP-102
HIS-100
GLY-22
GLY-20
ILE-19
VAL-27
Gln103
Asp102
Val101
His100
Ile19
Leu152
Asp104
Asn150
Gly20
cmpd8
Gln149
Lys147
Gly22
Val27
Asp163

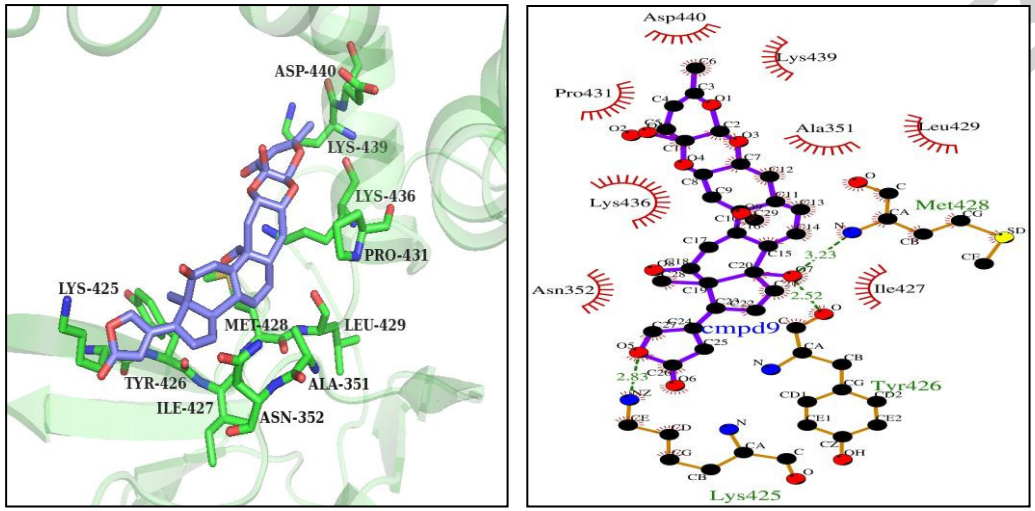
ASP-440
LYS-439
LYS-436
PRO-431
LYS-425
MET-428
LEU-429
TYR-426
ALA-351
ILE-427
ASN-352
Asp440
Lys439
Pro431
Ala351
Leu429
Lys436
Met428
Asn352
Ile427
cmpd9
Tyr426
Lys425

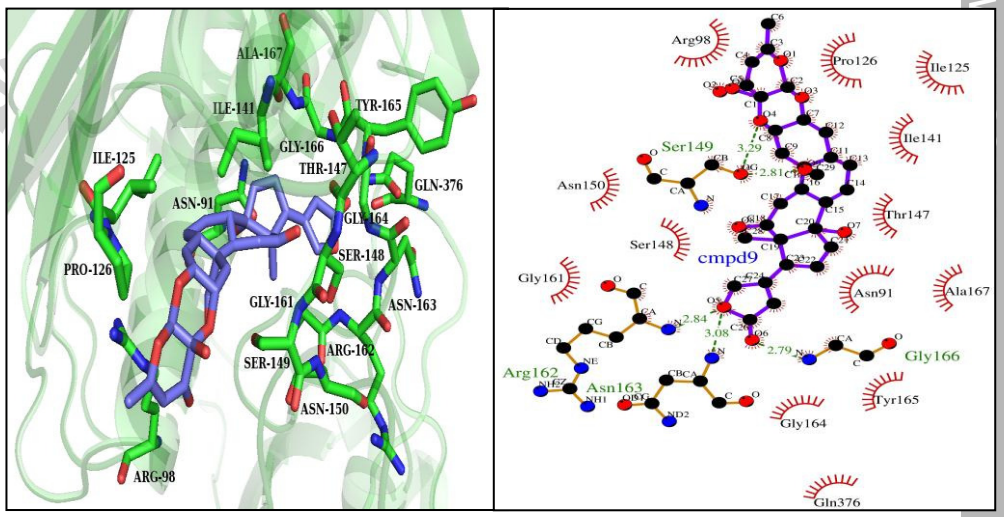
ALA-167
ILE-141
TYR-165
GLY-166
ILE-125
THR-147
GLN-376
ASN-91
GLY-164
SER-148
PRO-126
GLY-161
ASN-163
ARG-162
SER-149
ASN-150
ARG-98
Arg98
Pro126
Ile125
Ser149
Ile141
Asn150
Thr147
Ser148
cmpd9
Gly161
Asn91
Ala167
Gly166
Arg162
Asn163
Tyr165
Gly164
Gln376

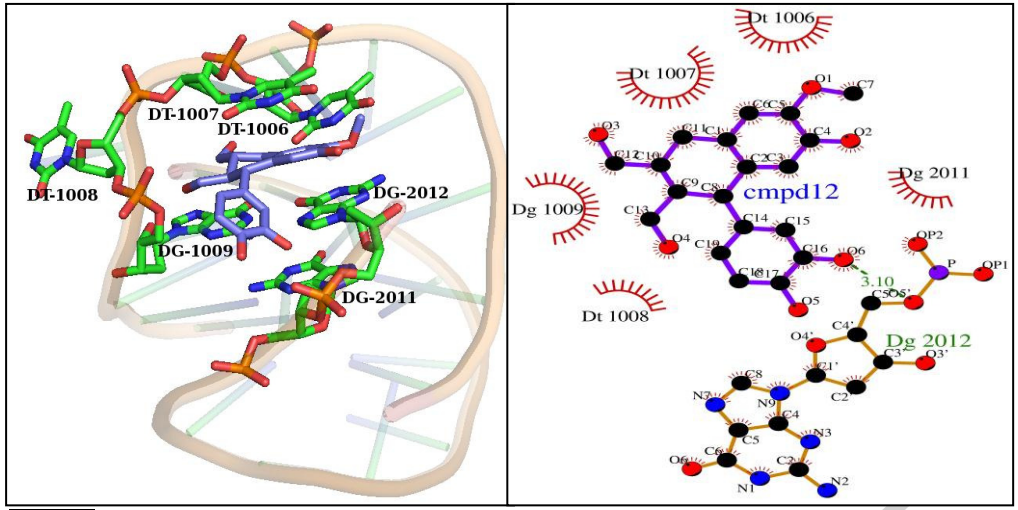
DT-1007
DT-1006
DT-1008
DG-2012
DG-1009
DG-2011
Dt 1006
Dt 1007
Dg 2011
Dg 1009
cmpd12
Dt 1008
Dg 2012
3.10

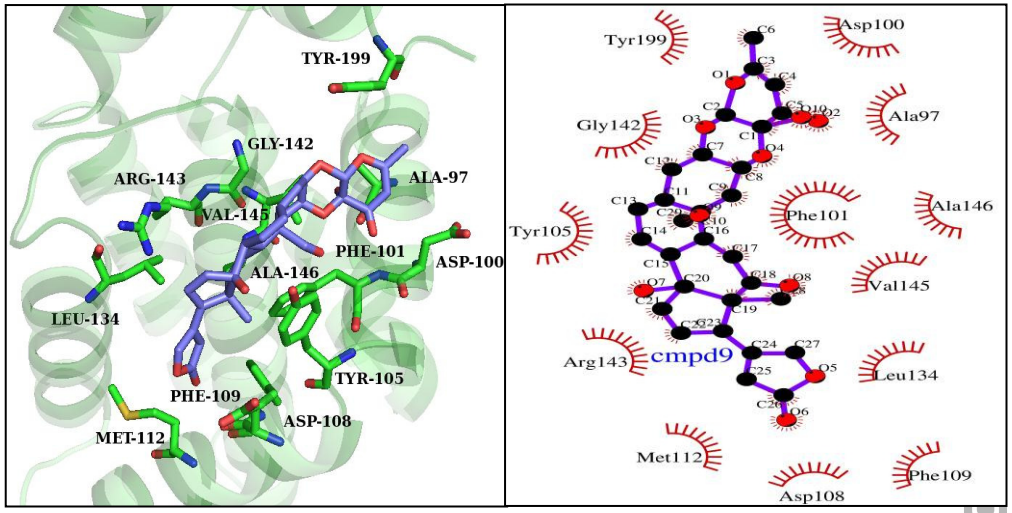
TYR-199
GLY-142
ARG-143
ALA-97
VAL-145
PHE-101
ASP-100
ALA-146
LEU-134
TYR-105
PHE-109
ASP-108
MET-112
Tyr199
Asp100
Gly142
Ala97
Ala146
Tyr105
Phe101
Val145
Arg143
cmpd9
Leu134
Met112
Phe109
Asp108

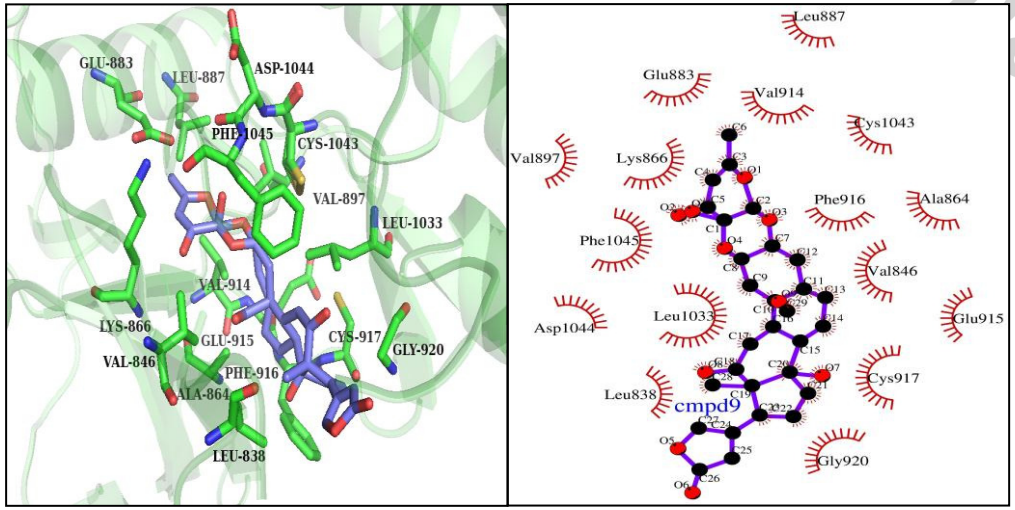
GLU-883
LEU-887
ASP-1044
PHE-1045
CYS-1043
VAL-897
LEU-1033
VAL-914
LYS-866
GLU-915
CYS-917
GLY-920
VAL-846
PHE-916
ALA-864
LEU-838
Leu887
Glu883
Val914
Cys1043
Val897
Lys866
Phe916
Ala864
Phe1045
Val846
Glu915
Asp1044
Leu1033
Leu838
cmpd9
Cys917
Gly920

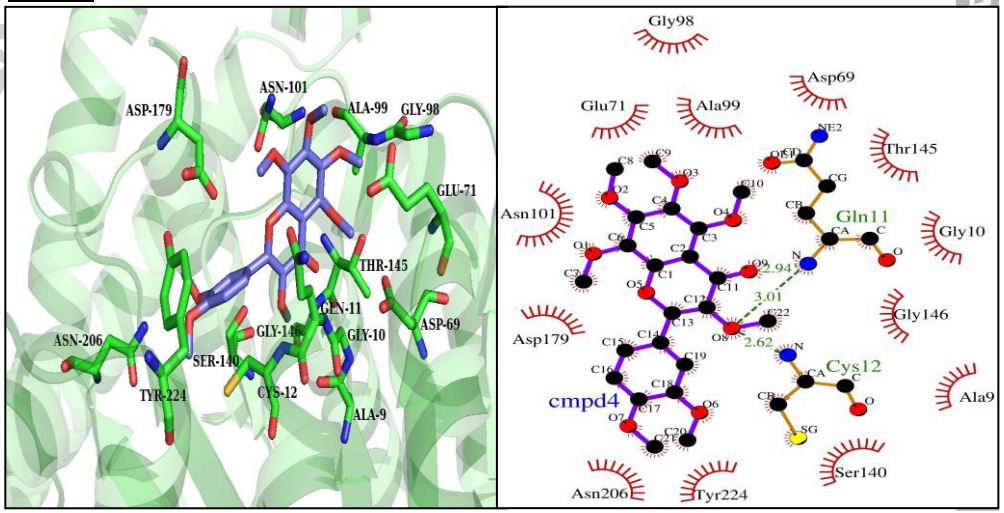
ASP-179
ASN-101
ALA-99
GLY-98
GLU-71
THR-145
GLN-11
ASP-69
ASN-206
SER-140
GLY-10
TYR-224
CYS-12
ALA-9
Gly98
Asp69
Glu71
Ala99
Thr145
Asn101
Gln11
Gly10
2.94
3.01
Gly146
Asp179
2.62
Cys12
cmpd4
Ala9
Asn206
Tyr224
Ser140

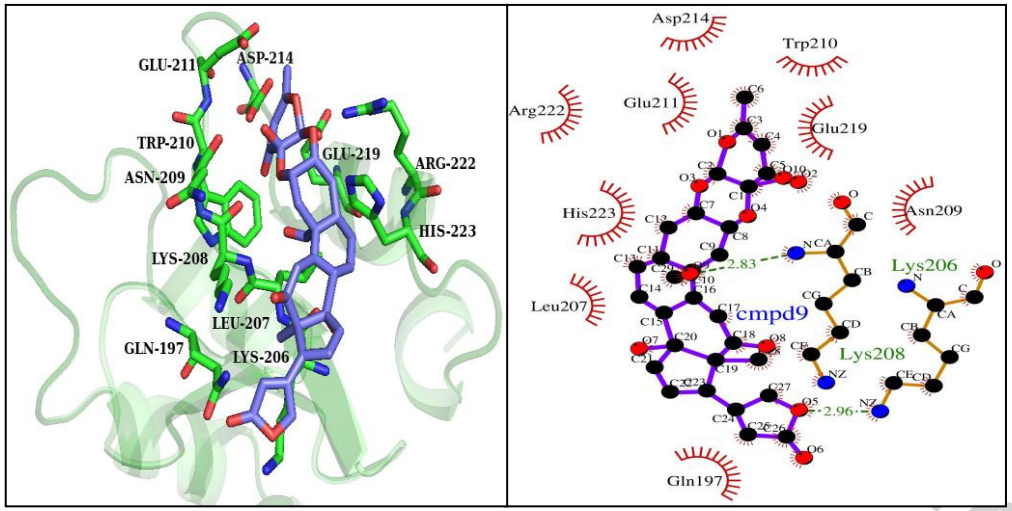

Figure 3

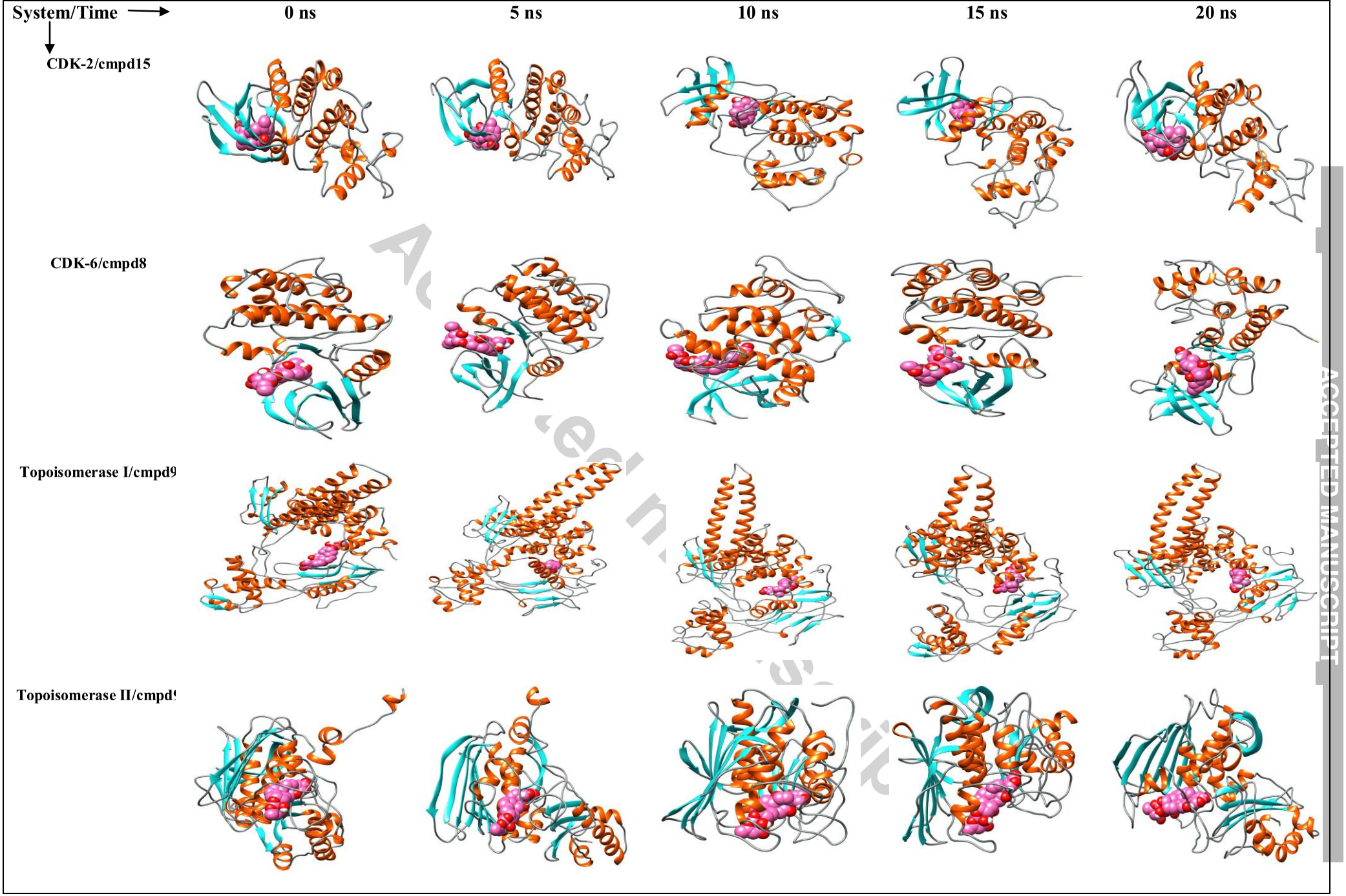

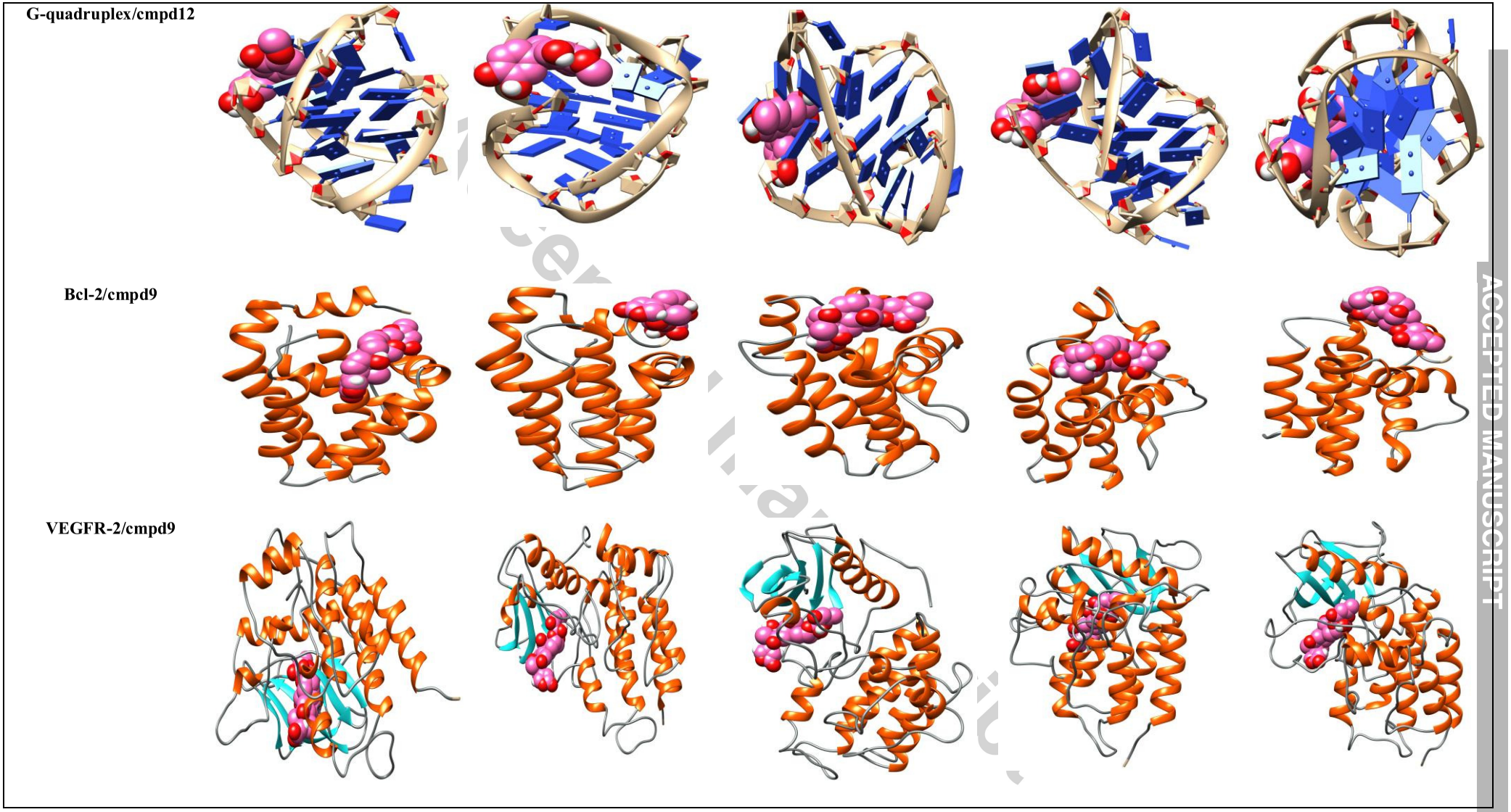

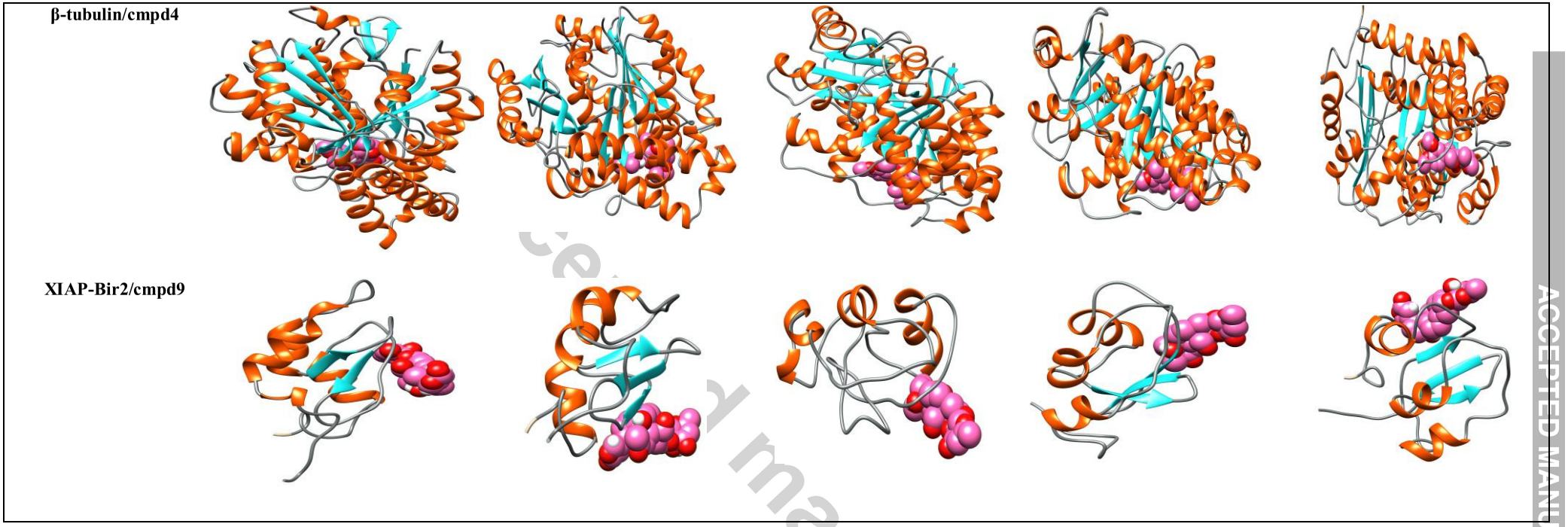

Figure 4

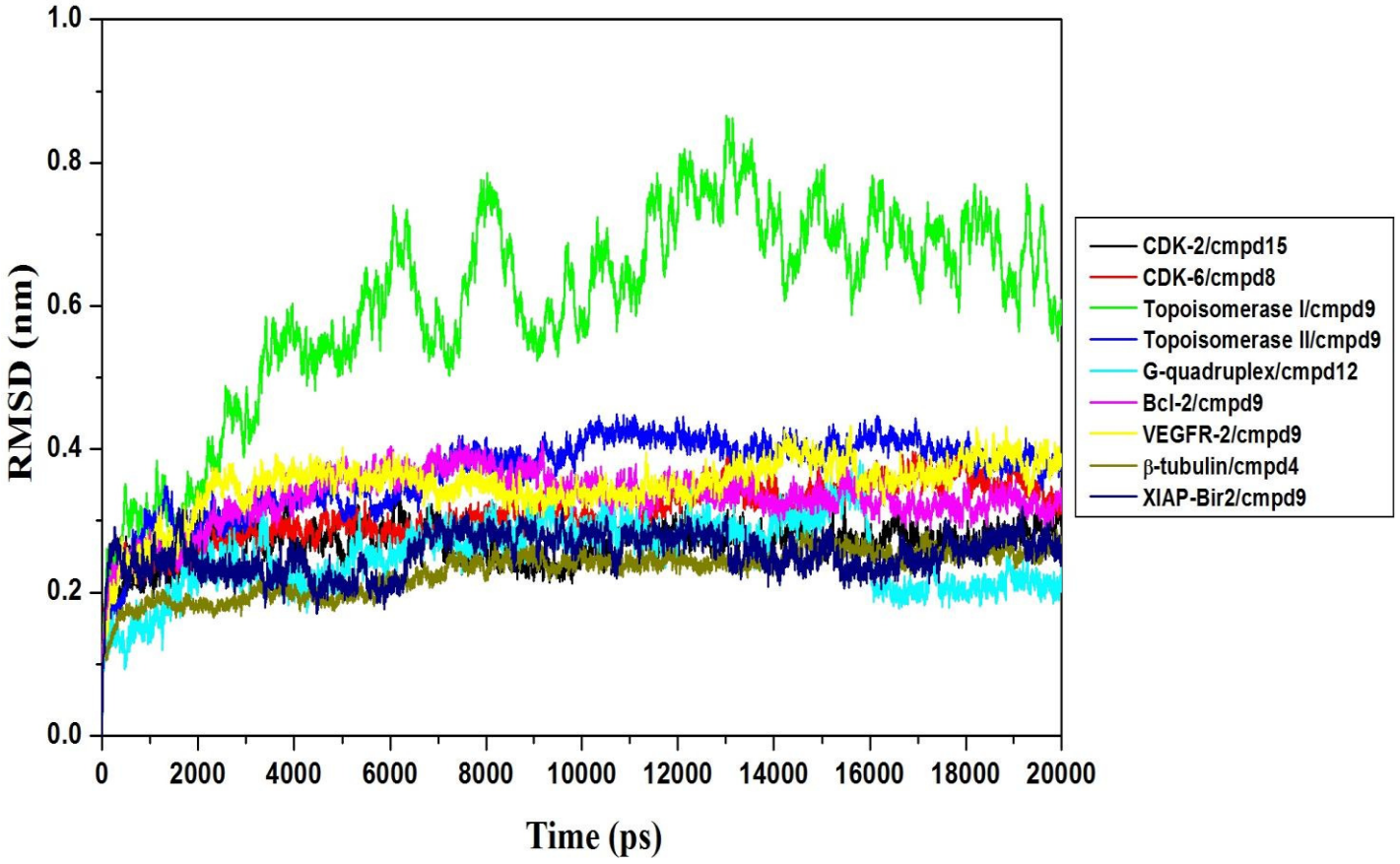

Figure 5

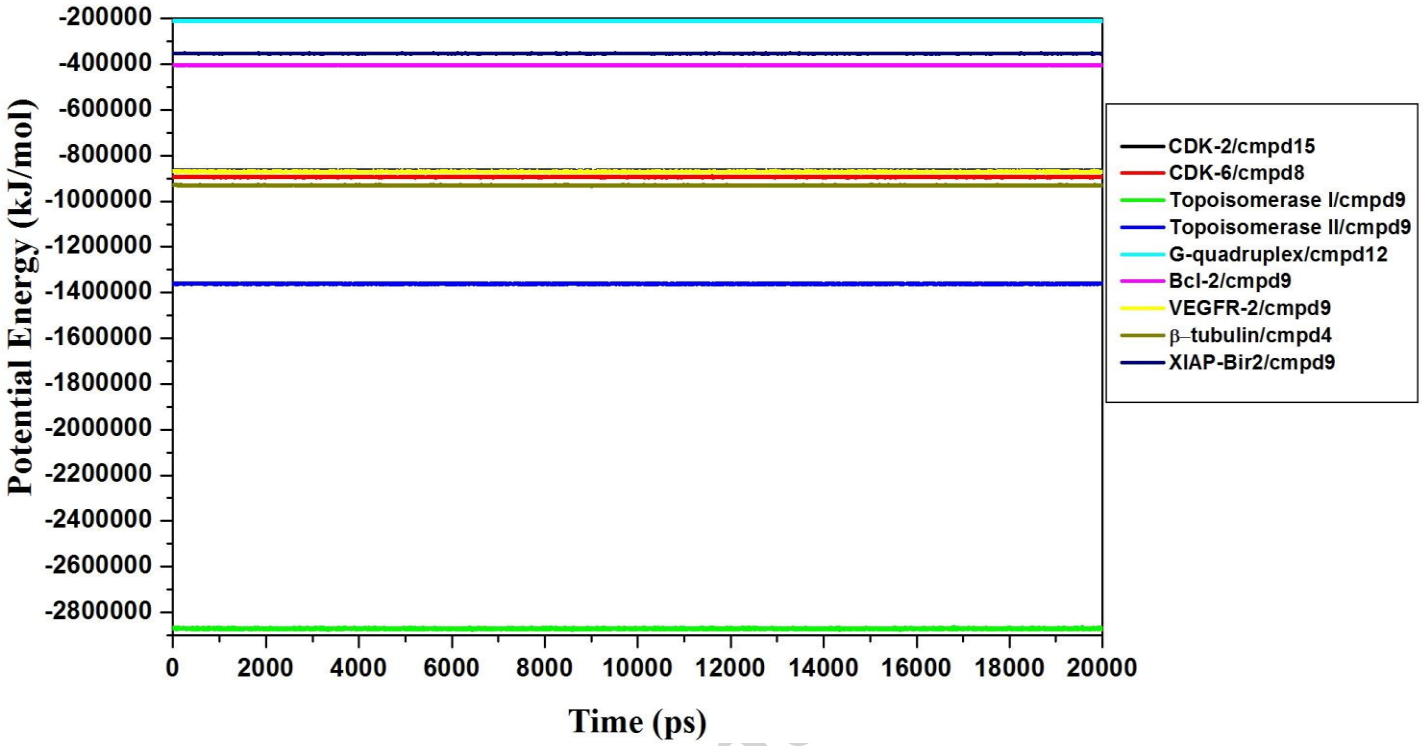

Figure 6

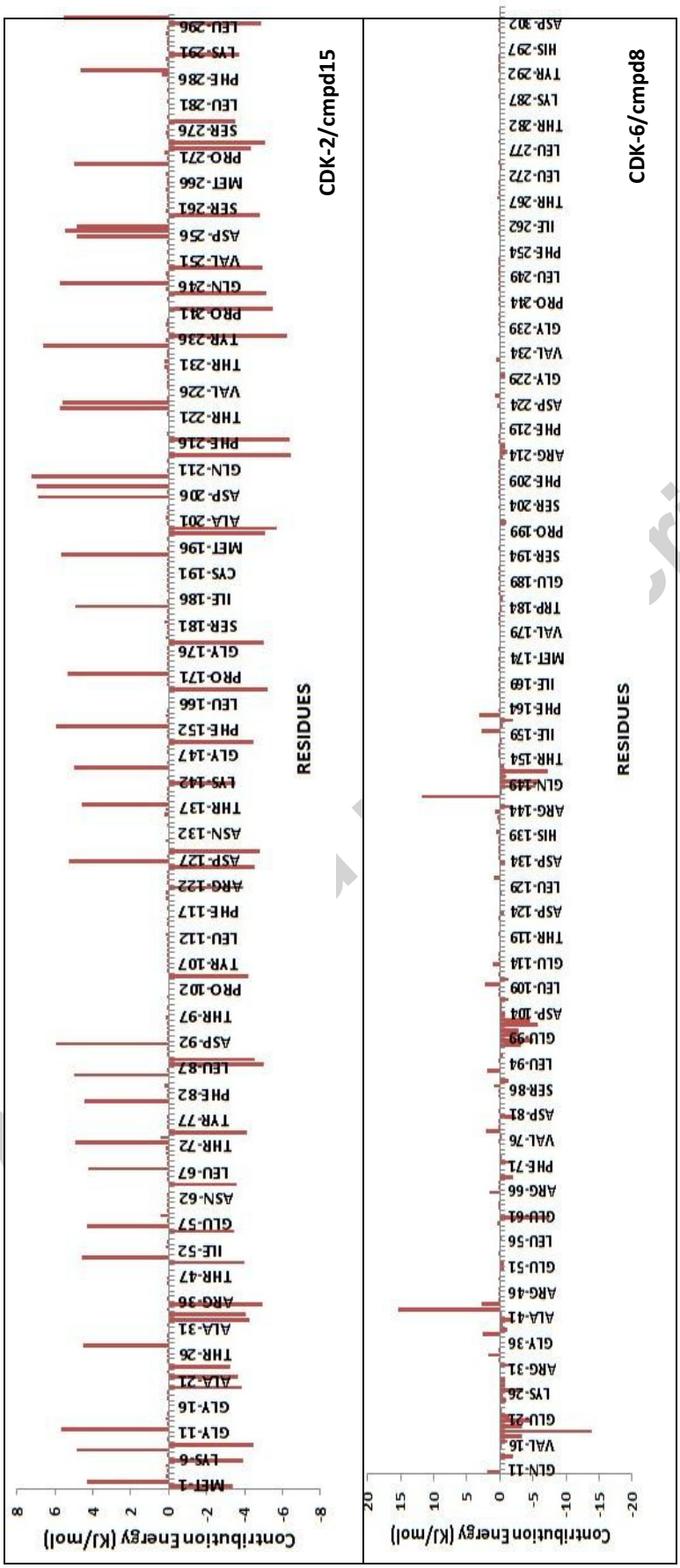

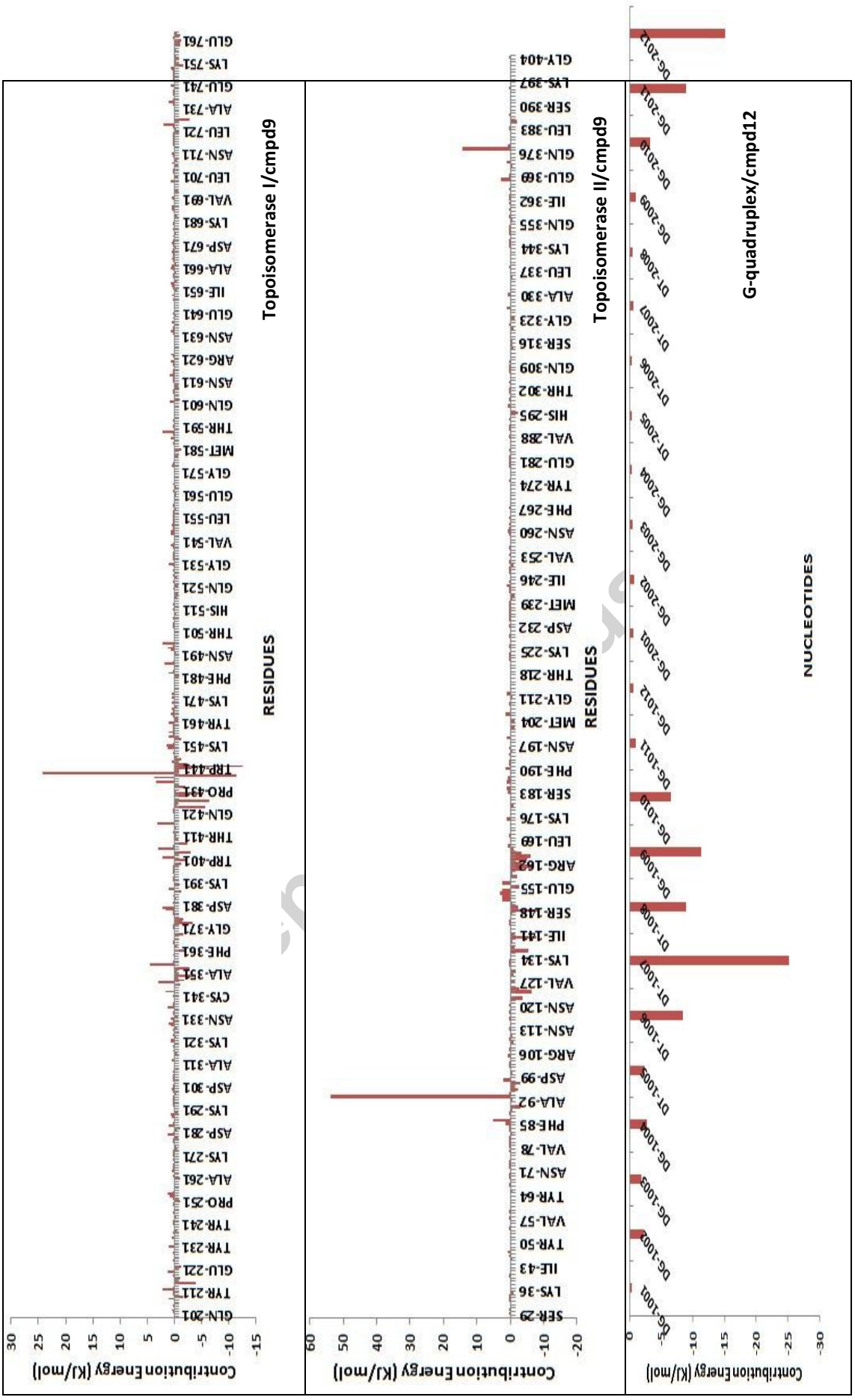

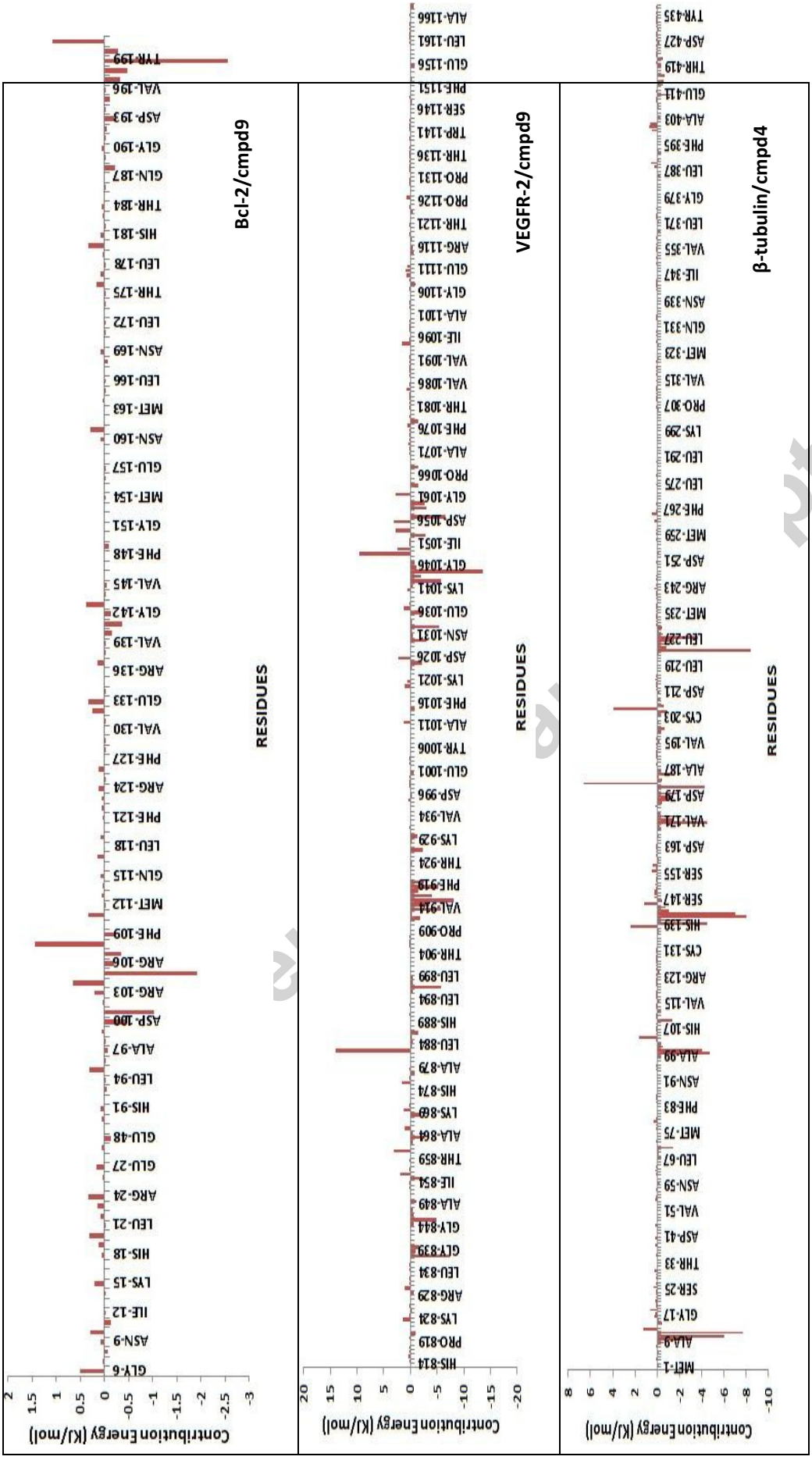

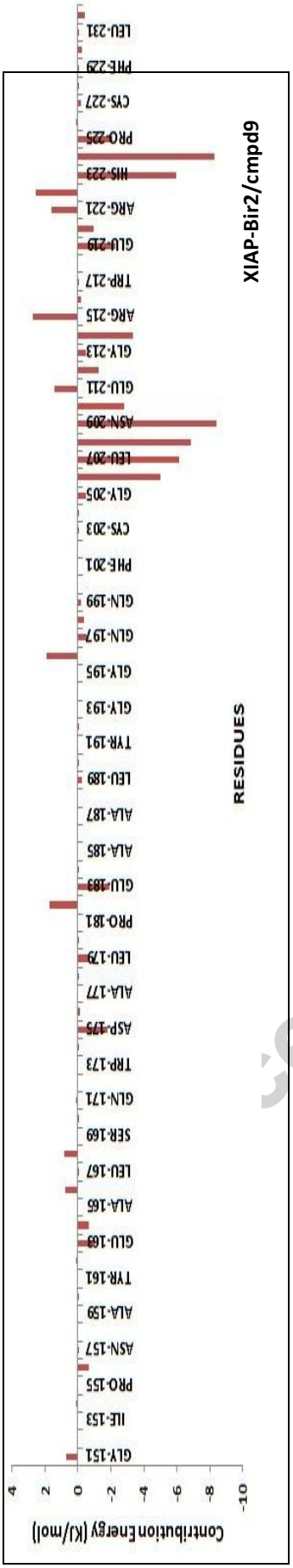

Figure 7

Table 1: The dimensions of grid box from the centre of bound ligands utilized for molecular docking studies.

Macromolecular target	Co-crystal ligand	Structure	Grid box dimensions		
			No. of grid points (npts)	Center (xyz coordinates)	Grid point Spacing (Å)
CDK-2	4-[3-Hydroxyanilino]-6,7-Dimethoxyquinazoline (DTQ)	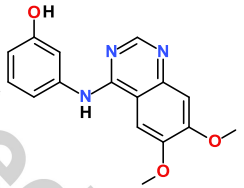	60× 60× 60	-7.623, 49.881, 11.367	0.375
CDK-6	3,7,3',4'-Tetrahydroxyflavone (FSE)	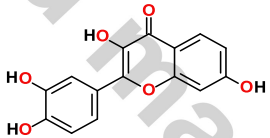	60× 60× 60	2.296, 36.095, 138.519	0.375
Topoisomerase I	4-Ethyl-4-Hydroxy-1,12-Dihydro-4h-2-Oxa-6,12a-Diaza-Dibenzo[B,H]Fluorene-3,13-Dione (EHD)	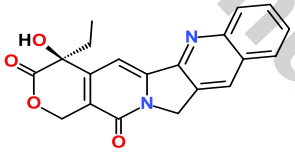	70× 70× 70	21.171, -3.904, 25.952	0.375

Topoisomerase II	Phosphoaminophosphonic Acid-Adenylate Ester (ANP)	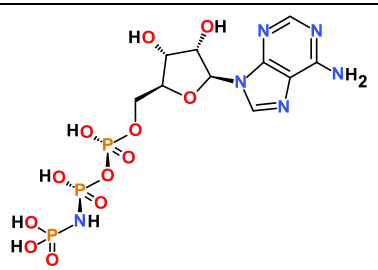	60× 60× 60	39.262, -1.072, 37.077	0.375
G-quaruplex	3-Pyrrolidin-1-Yl-N-[6-(3-Pyrrolidin-1-Yl-Propionylamino)-Acridin-3-Yl]-Propionamide (PYN)	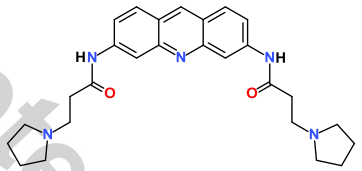	45× 45× 60	15.456, 16.903, 7.206	0.375
Bcl-2	4-(4-Benzyl-4-Methoxypiperidin-1-Yl)-N-[(4-{[1,1-Dimethyl-2-(Phenylthio)Ethyl]Amino}-3-Nitrophenyl)Sulfonyl]Benzamide (LI0)	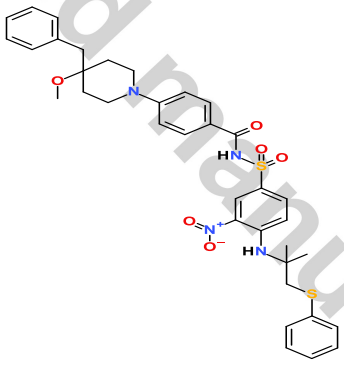	65× 65 ×65	-0.024, 3.142, -0.361	0.375
VEGFR-2	Methyl (5-{4-[({[2-Fluoro-5-(Trifluoromethyl)Phenyl]Amino}Carbonyl)Amino]Phenoxy}-1h-Benzimidazol-2-Yl)Carbamate (GIG)	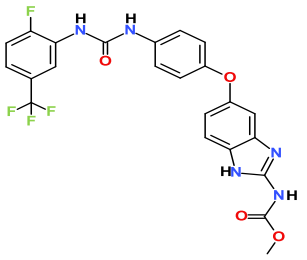	70× 70× 70	5.396, 32.493, 15.884	0.375

β-tubulin	Guanosine -5'-Diphosphate (GDP)	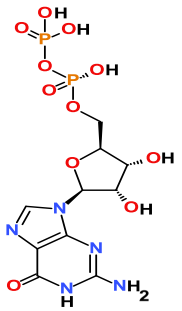	50× 50 ×50	14.662, 49.445, 18.869	0.375
XIAP-Bir2	N-{(3S)-5-(4-aminobenzoyl)-1-[(2-methoxynaphthalen-1-yl)methyl]-2-oxo-2,3,4,5-tetrahydro-1H-1,5-benzodiazepin-3-yl}-N~2~-methyl-L-alaninamide (1RH)	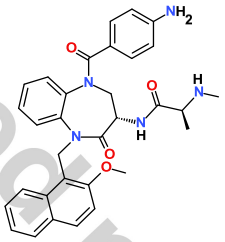	50 ×50× 50	29.799, 34.241, 11.358	0.375

Table 2: Physico-chemical conditions set for Molecular dynamics simulation of nine docked complexes.

Docked complexes	No. of residues/Nucleotides	Total charge on macromolecular targets	No. of water molecules	Counter ions added	Density(Kg/m^3)	Pressure(bar)	Temperature(K)
CDK-2/cmpd15	283	6.000 e	19932	6 Cl^- ions	999.661±0.17	0.931±0.32	299.647±0.27
CDK-6/cmpd8	289	-7.000 e	20610	7 Na^+ ions	999.358±0.098	1.006±0.17	299.72±0.28
Topoisomerase I/cmpd9	565	22.000 e	66655	22 Cl^- ions	992.761±0.096	1.009±0.075	299.667±0.37
Topoisomerase II/cmpd9	373	5.000 e	31402	5 Cl^- ions	997.745±0.14	0.966± 0.36	299.666±0.32
G-quaruplex/cmpd12	24	-22.000 e	4301	22 Na^+ ions	1031.57±0.43	1.164±1.2	299.906±0.13
Bcl-2/cmpd9	138	-5.000 e	9187	5 Na^+ ions	1004.18±0.29	1.287±0.97	299.718±0.2
VEGFR-2/cmpd9	299	2.000 e	19950	2 Cl^- ions	1003.1±0.15	1.139±0.37	299.707±0.34
β-tubulin/cmpd4	420	-15.000 e	20946	15 Na^+ ions	1011.27±0.1	0.890±0.23	299.73±0.26
XIAP-Bir2/cmpd9	82	1.000 e	8208	1 Cl^- ions	996.698±0.2	1.007±0.36	299.716±0.25

Table 3: Binding free energies (BE) in kcal/mol and inhibition constant (K_i) in nM of selected fifteen plant derived compounds docked against selected molecular targets.

Targets / Ligands	CDK-2		CDK-6		Topisomerase I		Topoisomerase II		G-quadruplex		Bcl-2		VEGFR2		β-Tubulin		XIAP-Bir2	
	BE	K_i	BE	K_i	BE	K_i	BE	K_i	BE	K_i	BE	K_i	BE	K_i	BE	K_i	BE	K_i
Cmpd1	-7.33	4240	-8.34	773.21	-7.03	7060	-7.41	3680	-7.78	1970	-5.64	73910	-7.97	1440	-7.18	5480	-6.07	35390
Cmpd2	-7.16	5670	-7.58	2790	-7.47	3350	-6.70	12290	-8.11	1140	-6.08	34920	-8.49	593.87	-6.43	19460	-6.21	27860
Cmpd3	-6.64	13550	-7.46	3390	-6.24	26540	-6.47	18060	-7.19	5410	-5.84	52110	-7.44	3530	-6.75	11230	-4.40	598380
Cmpd4	-6.39	20810	-6.01	39270	-6.24	26670	-4.65	387860	-5.64	73220	-3.97	1240000	-6.30	24050	-8.00	1370	-4.63	403530
Cmpd5	-6.67	12980	-7.72	2180	-6.23	27090	-5.42	106370	-8.17	1030	-4.48	521480	-8.04	1290	-6.83	9840	-4.89	259080
Cmpd6	-6.80	10330	-8.03	1300	-6.85	9450	-6.10	33700	-7.88	1690	-4.23	796240	-7.83	1830	-6.53	16350	-5.18	158290
Cmpd7	-5.53	88680	-5.38	114190	-6.15	31090	-5.31	128780	-6.66	13170	-6.00	39730	-6.58	14950	-5.22	149240	-5.03	206880
Cmpd8	-10.17	35.26	-11.09	7.48	-10.22	32.40	-8.93	285.08	-6.10	34050	-8.56	534.09	-10.37	24.86	-6.12	32550	-7.23	4980
Cmpd9	-10.58	17.43	-10.04	44.06	-10.87	10.69	-11.71	2.63	-6.85	9460	-9.46	117.15	-10.72	13.76	-7.26	4790	-8.34	773.40
Cmpd10	-9.21	176.46	-5.89	48200	-10.63	16.10	-8.14	1080	-4.47	531090	-7.52	3070	-7.30	4450	+30.31	-	-5.73	62650
Cmpd11	-8.01	1350	-8.70	421.66	-7.75	2080	-7.61	2620	-7.70	2270	-5.53	88320	-7.79	1960	-7.51	3140	-6.13	32210
Cmpd12	-7.89	1640	-9.79	66.40	-7.53	3040	-7.23	5020	-8.18	1010	-6.34	22620	-7.16	5640	-7.86	1720	-5.60	78030
Cmpd13	-6.86	9370	-7.20	5310	-6.05	37010	-5.82	54410	-6.19	29220	-4.12	961520	-7.17	5590	-7.04	6940	-4.25	771790
Cmpd14	-9.22	175.18	-8.07	1210	-8.38	714.73	-9.53	103.80	-4.82	294420	-7.98	1410	-7.58	2770	-5.39	111100	-6.73	11650
Cmpd15	-10.96	9.24	-6.10	33680	-9.16	194.20	-6.37	21430	-5.78	57510	-8.13	1090	-7.69	2290	-5.14	170000	-7.22	5140
Co-crystal ligands	-8.04	1280	-10.19	33.67	-10.75	13.27	-10.10	39.20	-11.54	3.50	-10.80	12.07	-12.32	0.931	-8.29	834.41	-9.39	130.57

Table 4: MM/PBSA binding free energies (KJ/mol) and their energy components for docked complexes calculated during the equilibration period.

Systems	Van der Waals energy (kJ/mol)	Electrostatic energy (kJ/mol)	Polar solvation energy (kJ/mol)	SASA energy (kJ/mol)	Binding free energy (kJ/mol)
CDK-2/cmpd15	-0.004±0.000	-57.472±0.155	25.427±1.751	0.085±0.099	-31.949±1.645
CDK-6/cmpd8	-233.213±0.696	-81.831±0.905	201.767±1.041	-19.542±0.036	-132.852±0.783
Topoisomerase I/cmpd9	-162.967±0.453	-109.155±1.268	210.465±1.971	-14.063±0.032	-75.686±0.811
Topoisomerase II/cmpd9	-245.002±0.544	-216.552±0.962	401.463±1.643	-20.288±0.040	-80.373±0.911
G-quadruplex/cmpd12	-186.012±0.837	-46.799±0.922	80.496±0.904	-16.122±0.035	-168.411±0.935
Bcl-2/cmpd9	-22.064±1.514	-16.906±1.104	40.005±1.824	-1.940±0.150	-0.840±1.172
VEGFR-2/cmpd9	-252.638±0.477	-172.578±0.950	328.935±1.514	-20.605±0.035	-116.953±0.718
β-tubulin/cmpd4	-271.204±0.389	-33.721±0.228	116.170±0.414	-19.065±0.029	-207.842±0.417
XIAP-Bir2/cmpd9	-155.453±1.043	-108.967±0.951	161.153±1.514	-11.920±0.065	-115.158±1.308

Table 5: The binding free energy contribution per residue wise of nine docked complexes. The figures in parentheses indicate binding energy contribution (kJ/mol).

Complexes	Binding free energy contribution per residue wise
CDK-2/cmpd15	Arg214 (-6.418±0.029), Arg217 (-6.407±0.032), Lys237 (-6.215±0.062), Arg200 (-5.707±0.025), Lys242 (-5.498±0.065), Arg169 (-5.202±0.025), Arg245 (-5.136±0.023), Arg199 (-5.095±0.025), Arg274 (-5.056±0.015), Lys178 (-5.029±0.066) and Lys88 (-5.025±0.053)
CDK-6/cmpd8	Ile19 (-13.972±0.072), Glu61 (-7.512±0.087), Leu152 (-7.185±0.059), Asn150 (-5.768±0.064), Asp102 (-5.687±0.078), Gln149 (-5.471±0.076) and Glu99 (-5.048±0.038)
Topoisomerase I/cmpd9	Lys443 (-12.498±0.203), Lys439 (-11.487±0.261), Met428 (-6.355±0.078), Lys425 (-5.712±0.113) and Pro431 (-5.257±0.047)
Topoisomerase II/cmpd9	Ser149 (-8.684±0.117), Ile141 (-7.953±0.038), Arg162 (-7.187±0.059), Ile125 (-6.587±0.036) and Val137 (-5.286±0.037)
G-quadruplex/cmpd12	Dt1007 (-25.171±0.126), Dg2012 (-15.050±0.136), Dg1009 (-11.262±0.192), Dt1008 (-8.928±0.114), Dg2011 (-8.904±0.069), Dt1006 (-8.385±0.131) and Dg1010 (-6.507±0.069)
Bcl-2/cmpd9	Tyr199 (-2.551±0.180), Tyr105 (-1.928±0.160), Phe101 (-1.030±0.072), Leu198 (-0.469±0.046), Asp100 (-0.429±0.040)
VEGFR-2/cmpd9	Phe1045 (-13.630±0.067), Phe916 (-8.146±0.048), Leu838 (-7.452±0.064), Tyr1057 (-6.547±0.160), Val914 (-5.776±0.036), Cys1043 (-5.75±0.048), Val897 (-5.727±0.034), Leu1033 (-5.392±0.043) and Phe919 (-5.302±0.095)
β-tubulin/cmpd4	Tyr224 (-8.373±0.095), Gly142 (-8.006±0.061), Cys12 (-7.724±0.063), Gly143 (-7.061±0.043) and Gln11 (-6.068±0.059)
XIAP-Bir2/cmpd9	Asn209 (-8.393±0.116), Phe224 (-8.29±0.092), Lys208 (-6.88±0.237), Leu207 (-6.157±0.047) and His223 (-5.955±0.099)

Table 6: Physicochemical properties of selected plant derived compounds calculated using Molinspiration.

Compounds	Name	LogP[a]	MW[b]	HBA[c]	HBD[d]	nviolations[e]
Cmpd1	acetylshikonin	2.26	316.31	6	2	0
Cmpd2	5,7,4'-Trimethoxyflavanone	3.26	314.34	5	0	0
Cmpd3	3-(8'(Z),11'(Z)-pentadecadienyl)catechol	7.38	316.49	2	2	1
Cmpd4	3,5,6,7,8,3',4'-heptamethoxyflavone	3.35	432.43	9	0	0
Cmpd5	Chrysoplenetin	2.59	374.35	8	2	0
Cmpd6	Chrysosplenol	2.28	360.32	8	3	0
Cmpd7	1-phenyl-hepta-1,3,5-triyne	3.71	164.21	0	0	0
Cmpd8	Asclepin	1.85	574.67	10	2	1
Cmpd9	12B-hydroxycalotropin	0.23	548.63	10	4	1
Cmpd10	Solamargine	2.41	868.07	16	9	3
Cmpd11	Taxiresinol	2.02	346.38	6	4	0
Cmpd12	Isotaxirenisol	1.32	346.38	6	5	0
Cmpd13	Secoisolariciresinol	2.08	362.42	6	4	0
Cmpd14	2-deacetoxytaxinine J (2-DAT-J)	7.25	650.76	10	0	2
Cmpd15	Asiatic acid	4.7	488.71	5	4	0

a: Partition coefficient between n-octanol and water, b: Molecular weight, c: Hydrogen bond acceptor, d: Hydrogen bond donor, e: Number of ROF violations

Table 7: Physicochemical properties of selected plant derived compounds calculated using DataWarrior.

Compounds	cLogS[a]	PSA (Å^2)[b]	RB[c]	Druglikeness	Mutagenic	Tumorigenic	Reproductive Effective	Irritant
Cmpd1	-1.898	100.9	6	-2.3149	low	low	none	none
Cmpd2	-3.582	53.99	4	-0.13101	none	none	none	none
Cmpd3	-4.581	40.46	12	-14.789	none	none	none	high
Cmpd4	-3.83	94.82	9	1.6253	none	none	none	none
Cmpd5	-3.184	107.59	6	-0.54261	none	none	none	none
Cmpd6	-2.87	118.59	5	0.21649	none	none	none	none
Cmpd7	-7.283	0	3	-7.4721	none	high	none	none
Cmpd8	-4.757	137.82	4	-2.4127	none	none	none	none
Cmpd9	-3.948	151.98	2	-2.5188	none	none	none	none
Cmpd10	-5.557	238.48	7	3.1642	none	none	low	none
Cmpd11	-2.163	99.38	5	-0.47393	none	none	none	none
Cmpd12	-2.293	110.38	4	-3.9043	none	none	none	none
Cmpd13	-2.544	99.38	9	-3.9043	none	none	none	none
Cmpd14	-6.344	131.5	12	-5.1523	none	none	none	high
Cmpd15	-5.205	97.99	2	-5.9983	none	none	none	none

a: Aqueous solubility at 25^o and pH=7.5, b: Polar surface area , c: Rotatable bonds

Table 8: Drug-like properties of selected natural compounds calculated using FAF Drugs3.

Compounds	Oral bioavailability (VEBER)	Oral bioavailability (EGAN)	Phospho-lipidosis	Fsp^{3a}
Cmpd1	Good	Good	NonInducer	0.24
Cmpd2	Good	Good	NonInducer	0.28
Cmpd3	Good	Good	NonInducer	0.52
Cmpd4	Good	Good	NonInducer	0.32
Cmpd5	Good	Good	NonInducer	0.21
Cmpd6	Good	Good	NonInducer	0.17
Cmpd7	Good	Good	NonInducer	0.08
Cmpd8	Good	Good	NonInducer	0.84
Cmpd9	Good	Good	NonInducer	0.86
Cmpd10	Good	Good	Inducer	0.96
Cmpd11	Good	Good	NonInducer	0.37
Cmpd12	Good	Good	NonInducer	0.37
Cmpd13	Good	Good	NonInducer	0.4
Cmpd14	Good	Good	NonInducer	0.54
Cmpd15	Good	Good	NonInducer	0.9

a: Number of sp^3 hybridized carbons/total carbon count

Table 9: Adsorption, Distribution Metabolism Excretion and Toxicity (ADMET) properties of selected plant derived compounds calculated using PreADMET.

Compounds	BBB[a]	HIA[b]	CYP_2C19_inhibition[c]	Pgp_inhibition[d]	Plasma_Protein_Binding
Cmpd1	0.063	90.239	Inhibitor	Non	87.659
Cmpd2	1.240	98.069	Inhibitor	Non	89.692
Cmpd3	14.716	93.527	Inhibitor	Inhibitor	100
Cmpd4	0.069	98.954	Inhibitor	Inhibitor	75.996
Cmpd5	0.015	93.076	Inhibitor	Non	78.126
Cmpd6	0.040	86.802	Inhibitor	Non	78.556
Cmpd7	3.552	100	Inhibitor	Non	100
Cmpd8	0.015	89.322	Non	Inhibitor	76.883
Cmpd9	0.039	71.437	Non	Non	49.998
Cmpd10	0.036	23.394	Non	Inhibitor	36.766
Cmpd11	0.315	83.048	Inhibitor	Non	87.496
Cmpd12	0.101	73.963	Inhibitor	Non	89.916
Cmpd13	0.398	84.137	Inhibitor	Non	87.816
Cmpd14	0.351	99.748	Inhibitor	Inhibitor	90.727
Cmpd15	0.628	91.239	Non	Inhibitor	96.455

a: Brain barrier penetration, b: Human intestinal absorption , c: Cytochrome P450 (CYP) enzyme, d: P-glycoprotein inhibition